AD-A080 179 AIR FORCE INST OF TECH WRIGHT-PATTERSON AFB OH SCHOO--ETC F/G 7/4
THE VALIDITY OF VELOCITY CALCULATIONS BASED ON THE PLUG FLOW AS--ETC(U)
DEC 79 P J WOLF
UNCLASSIFIED AFIT/GEP/PH/79D-14 NL

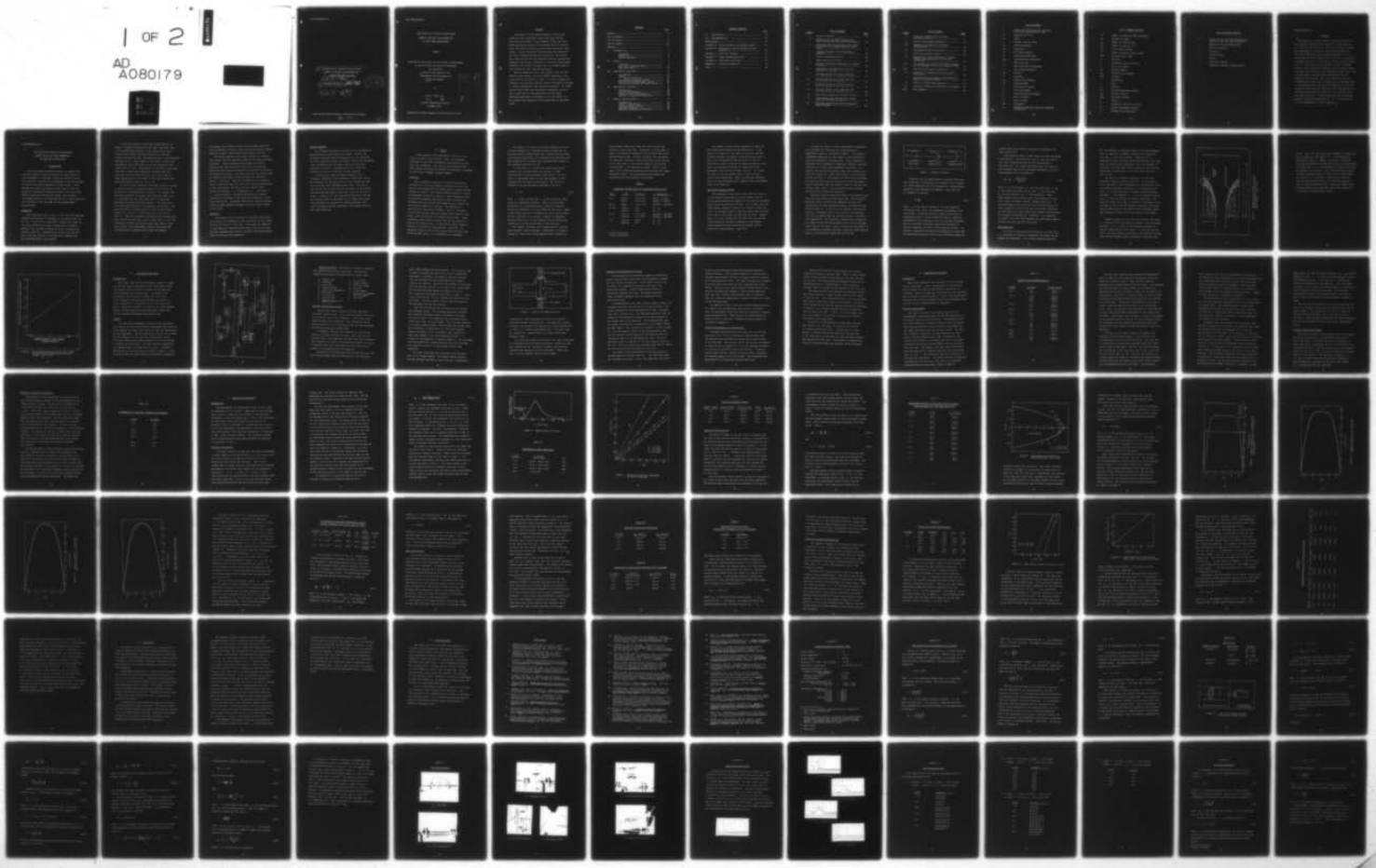

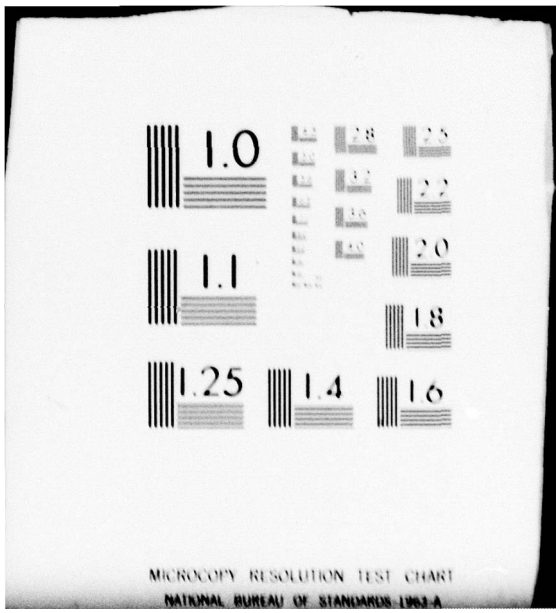
1.0
1.1
1.25
1.4
1.6
2.0
2.2
2.5
2.8
3.2
3.6
4.0
18
MICROCOPY RESOLUTION TEST CHART
NATIONAL BUREAU OF STANDARDS 1963 A

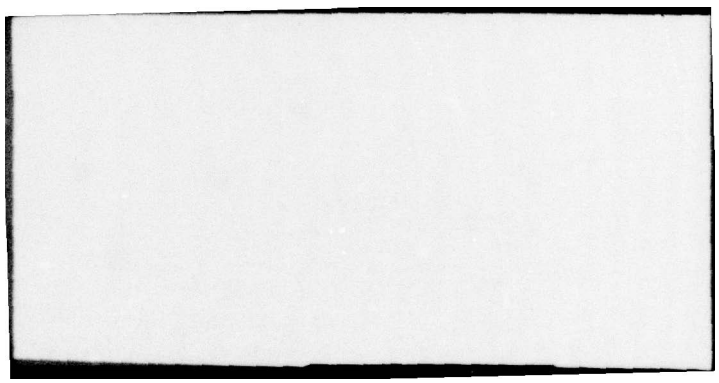

AFIT/GEP/PH/79D-14

(6) THE VALIDITY OF VELOCITY CALCULATIONS BASED ON THE PLUG FLOW ASSUMPTION IN FLOW TUBE APPLICATIONS.

(9) Master's THESIS,

(14) AFIT/GEP/PH/79D-14

(10) Paul J. Wolf
2D Lt USAF

(11) Dec 79

(12) 98

012 225

mt

AFIT/GEP/PH/79D-14

THE VALIDITY OF VELOCITY CALCULATIONS BASED ON THE PLUG FLOW ASSUMPTION IN FLOW TUBE APPLICATIONS

THESIS

Presented to the Faculty of the School of Engineering
of the Air Force Institute of Technology
Air University
in Partial Fulfillment of the
Requirements for the Degree of
Master of Science

by

Paul J. Wolf, B.S.
2D Lt USAF
Graduate Engineering Physics

December 1979

Preface

The results of this study presented in this paper should aid many researchers using flow tubes when gas velocities are needed. In my research I found that many people quoted gas velocities in various flow tube applications, but with no mention as to how they arrived at those values. I later discovered that the plug flow assumption was used to calculate these gas velocities. The problem that arose was how well the plug flow velocity calculations represent the true gas velocities in flow tube applications. Therefore, this study is unique since no in-depth study of this problem has been examined previously.

Special thanks are due to Dr. Steven J. Davis of the Chemical Laser Branch, Air Force Weapons Laboratory, and to my advisor, Dr. Ernest A. Dorko. Dr. Davis brought this problem to my attention, and has offered invaluable assistance in solving experimental and theoretical problems. Dr. Dorko supplied much advice on experimental techniques, and has been a great help in the preparation of this paper. Additional gratitude is expressed to my wife, Kathy, for her patience and endurance in the preparation of the first draft.

Contents

Contents (Cont'd)

List of Figures

List of Tables

List of Symbols

A	Transition probability for emission; flow tube cross-sectional area
Å	Angstrom (10^{-8} cm)
Ar	Argon
c	Concentration of atoms
cc	Cubic centimeters
cm	Centimeter
D	Flow tube diameter
D′	Diffusion coefficient
D_{11}	Self-diffusion coefficient
F	Mass flow rate
F′	Mass flow rate in moles/sec
h	Step height parameter
Hg	Mercury
I	Intensity
I_n	Normalized intensity
Kn	Knudsen number
k	Boltzmann's constant
L	Flow tube length
L′	Recirculation zone length
m	Mass in g/mole
m′	Mass in grams
mm	Millimeters
N	Number of atoms that have not undergone a collision

List of Symbols (Cont'd)

N^*	Number of atoms per cubic centimeter
N_a	Avogadro's number
N_e	Number of excited atoms
N_o	Number of atoms at t = 0
N_T	Total number of atoms
n	Number of atoms per unit volume
PMT	Photomultiplier tube
p	Pressure
Q	Volumetric flow rate of air
R	Flow tube radius
Re	Reynolds number
R_o	Universal gas constant
std	standard
T	Temperature
t	Time
u	Velocity
$\langle u \rangle$	Average Maxwellian velocity
u_{av}	Average velocity
u_{pf}	Plug flow velocity
V	Volume
$\dot{V}$	Volumetric flow rate of argon
X_L	Laminar development length
x	Distance from electrodes

List of Symbols (Cont'd)

y	Heights in the flow tube measured with respect to the flow tube centerline
z	Number of collisions per second
Γ	Rate of transport
η	Viscosity
λ	Mean free path
ρ	Density
σ	Collision diameter
τ	Radiative lifetime; shearing stress

AFIT/GEP/PH/79D-14

Abstract

The validity of linear velocity calculations based on the plug flow assumption were tested on flowing argon at 4.2, 5.0, 6.0, and 10.1 torr. The linear velocity of argon was experimentally determined along the centerline of a flow tube, using the argon afterglow technique. It was found that the linear velocity was 1.62 times the plug flow (average) velocity at a flow rate of 4576.0 standard cc/min and 1.77 times the plug flow velocity at 5262.4 standard cc/min. The velocity data taken at various distances from the centerline revealed a fully developed laminar flow. The velocity results differed from that predicted by the Poiseuille flow formula, and it was determined that this difference was mainly due to obstructions in the argon flow. It was concluded that the plug flow assumption can be used to obtain linear gas velocities in a fully developed laminar flow and approximate gas velocities if the laminar flow is not fully developed. A Stern-Volmer plot was constructed and the results indicated that the $^1D - {}^1S$ multiplet of Ar V was responsible for the afterglow.

AFIT/GEP/PH/79D-14

THE VALIDITY OF VELOCITY CALCULATIONS BASED ON THE PLUG FLOW ASSUMPTION IN FLOW TUBE APPLICATIONS

I. Introduction

One of the areas of recent interest in excited state chemistry and fast reaction kinetics has been centered on the development of electronic transition chemical lasers. This interest stimulated the development of specific methods to observe the various phenomena in these fields. These methods were tested on gaseous systems using an old, yet versatile, experimental apparatus called a flow tube (also known as fast-flow reactors and tubular flow reactors). The widespread use of the flow tube has led to many variations in the design to suit the needs of the problem under investigation.

Background

Flow tubes were used as early as 1910 when Lord Rayleigh examined the afterglow of nitrogen in a discharge (Refs 18, 24, 25). In the 1920's, Wood made a significant advance in flow tube technology by using a vacuum pump to withdraw products from a steady discharge to observe hydrogen atom reactions (Ref 32). Widespread use of flow tubes did not occur until the interest in excited state chemistry and fast reaction kinetics was aroused.

In reaction kinetics, flow tube systems provide the means to determine reaction rates of fast reactions. This can be accomplished because, in the flowing gas, little mixing occurs between reactants entering the tube and products leaving the tube. The determination of the mechanism and kinetics of a large number of fast atomic reactions at temperatures lower than 1000° K have been studied in this manner (Refs 20, 28). Improvements in flow tube systems have been made to study high temperature reactions (Ref 14) occurring in such systems as Fe/O_2 and Al/O_2 (Ref 12). Other applications of flow tubes in reaction kinetics have also been reported (Refs 3, 10, 27, 29).

In excited state chemistry, flow tubes provide the means to directly observe the electronically excited states of molecules in chemiluminescent reactions. For example, the radiative lifetimes of various metal fluorides (Refs 1, 2, 8), chlorides (Ref 33), and oxides (Ref 5) have been determined using emission spectroscopy. Flow tubes have also been used successfully in molecular spectroscopy. For example, Capelle and Brom reported a new GeO band system, namely, the $b^3\pi_1 \rightarrow X^1\Sigma^+$ system observed in the near uv (Ref 4). Other new molecular transitions and constants have been reported in many metal oxide systems (Refs 11, 15, 16). Furthermore, burners and furnaces have been added to flow tube systems. This advancement improved the methods for the production of diatomic metal oxides and halides.

West et al. have reported various furnace designs utilized in the production of metal vapors, and various burner designs employed in metal atom-oxidant mixing schemes (Ref 29).

The linear velocity of the gases flowing in a tubular flow reactor has been reported in many of the above mentioned references. These velocities were needed to calculate reaction rates and to provide a basis for a correlation between various physical parameters in different gas mixtures and chemical reactions. The velocities were calculated using an idealized flow model called the plug flow assumption (Refs 7, 9, and 29). Plug flow is defined as an idealized state of flow such that, over any cross-section perpendicular to the fluid motion, the mass flow rate and the fluid properties pressure, p, temperature, T, and density, ρ, remain constant. Extensive information is lacking concerning the validity of the plug flow assumption in flow tube applications. Swearengen (Ref 26) has reported limited results on this problem, although it was not a main concern of his study.

Objective

The purpose of this study was to determine the validity of the plug flow assumption in the calculation of the linear velocity of a gas in a flow tube. This study was completed by experimentally determining the linear velocity of a gas, and then comparing these results to that of the calculations based on the plug flow assumption.

General Approach

The afterglow technique was utilized in experimentally determining the linear velocity of argon. Briefly, the afterglow technique involves exciting a gas in a discharge such that metastable states are formed. When these metastable states recombine with the ground state via collisions, radiation is emitted. Afterglow then occurs when this radiation is in the visible part of the spectrum.

In this study, argon was passed through a spark discharge, resulting in the formation of metastable states. The afterglow was then detected at a point downstream from the electrodes with a photomultiplier tube. The time it took for the gas to flow from the electrodes to the observation point was measured by observing a pulse on an oscilloscope. A velocity was then calculated using this time and the distance from the electrodes to the observation point. This procedure was repeated for various pressures, flow rates, distances from the electrodes, and heights above the flow tube centerline.

II. Theory

A brief account of the theoretical aspects of this study is given in this section. First, the afterglow technique is discussed, followed by an explanation of the plug flow assumption. This section then concludes with some remarks concerning the problem of achieving a reattached gas flow with a suddenly expanded chamber.

Afterglow

When a potential difference is established between electrodes in a gas and gradually increased, little or no current flows between the electrodes until a sharply defined voltage is reached. This sharply defined voltage is called the breakdown potential of the gas. After breakdown occurs, an electric discharge takes place in which electrons are liberated from the cathode with enough energy to excite the gas passing through the discharge. The mechanism of excitation is collisional in nature. That is, electrons collide with the gas atoms and transfer their energy to the atoms, which are excited into higher energy states. After excitation, there exists a finite time for the species to decay to the ground state. As the species decay, energy is released in the form of electromagnetic radiation. If radiation occurs in the visible region after the decay time of the excited states, it is referred to as afterglow.

For example, the long lived yellow afterglow of active nitrogen produced by a discharge through nitrogen gas was discovered over a hundred years ago. Between 1910 and 1940, Lord Rayleigh showed that this afterglow was associated with the recombination of ground state nitrogen atoms formed in the discharge (Refs 18, 24, 25).

In rare gases, it is known that some of the lowest excited states are metastable and can exist in high concentrations in glow discharges (Ref 6:237). The lifetime of a metastable state is very long compared to the lifetime of a non-stable excited state. The radiative lifetime of an excited state is defined in Eq (2-1).

$$\tau = 1/A \qquad (2\text{-}1)$$

where τ is the lifetime and A is the transition probability for spontaneous emission. Thus, the transition probability of a metastable state is much less than the transition probability of a non-stable excited state. Atoms in metastable states can recombine with their ground states only by collisions if no external stimulus is supplied. Afterglow then occurs if the radiation emitted during this transition is in the visible part of the spectrum.

For example, afterglow can be demonstrated by passing argon through a spark discharge. Furthermore, if argon is flowing in a flow tube, the metastable states produced by

the discharge would travel down the tube with the same velocity as the argon flow. Therefore, it is possible to detect the afterglow downstream from the electrodes with a photomultiplier tube. In order to detect this afterglow, the radiative lifetimes of these metastable states must be of the same order as the time of flight of the gas from the electrodes to the observation point. Table I lists some of the transition probabilities associated with argon metastable states. The corresponding wavelengths and transitions are also included in the Table.

TABLE I

Transition Probabilities of Argon Metastable States[a]

Ion	λ (Å)	A (sec^{-1})	Transition
Ar I	5056.3	7.50×10^{4}	$4p[\frac{1}{2}]_1 - 7s\ [\frac{1}{2}]_0$
	6481.1	9.80×10^{4}	$4p[\frac{1}{2}]_0 - 7s\ [9/2]_1$
Ar II	6984.2	5.26×10^{-2}	$3p^5(^2P^0) - 3p^5(^2P^0)$
Ar III	3109.0	4.02	$^3P - {}^1S$
	5191.82	3.10	$^1D - {}^1S$
Ar IV	4711.33	8.0×10^{-2}	$3p^3(^4S^0) - 3p^3(^2D^0)$
	4740.20	7.2×10^{-3}	$3p^3(^4S^0) - 3p^3(^2D^0)$
Ar V	6435.10	0.223	$^3P - {}^1D$
	4625.54	3.8	$^1D - {}^1S$

[a] (Ref 31:202-224)

For example, typical linear velocities of gases in flow tubes range between 500 and 3000 cm/sec. If the velocity of argon in a flow tube is 700 cm/sec and the distance from the electrodes to the observation point is 30 cm, the corresponding time of flight is .043 sec. Therefore, in order to detect the argon afterglow at this point, the radiative lifetime of a particular argon metastable state must be at least .043 sec. It is seen that most of the metastable states listed in Table I satisfy this requirement. Thus, any afterglow detected due to an argon discharge must originate from a metastable state in an argon ion.

Plug Flow Assumption (PFA)

One advantage of the tubular flow reactor is that it can be operated continuously in such a manner that no mixing occurs between the elements of the fluid at different points along the direction of flow. In the ideal case, the fluid passes through the reactor in a process called plug flow. As the name suggests, plug flow means that the fluid moves like a solid plug or piston down the tube. Furthermore, it is also assumed that the mass flow rate and the fluid properties, pressure, temperature, and density, remain uniform over any cross-section normal to the direction of fluid motion. (Ref 7:36)

In practice, there is always some degree of departure from the plug flow conditions of uniform velocity, temperature, density, and pressure (Ref 9). For example, temperature gradients at right angles to the direction of flow cause deviations from plug flow. These temperature gradients can be produced in combustible chemical reactions, resulting in a flame (chemiluminescent reactions). For example, the reaction of germane, GeH_4, plus fluorine in a flow tube results in a flame which contains electronically excited GeF (Ref 1). The products of this reaction leaving the reaction zone along the centerline of the flame have a higher temperature than the products closer to the walls of the flow tube. Thus, a cooling problem exists to bring the flow close to plug flow conditions.

Extensive velocity gradients normal to the direction of flow also cause deviations from plug flow. These velocity gradients can be visualized by comparing the plug flow profile with the fully developed laminar and turbulent flow profiles (Fig. 1). If the flow is turbulent, the velocity profile is reasonably flat in the region of the turbulent core, but in laminar flow the velocity profile is parabolic (see Appendix B). This parabolic velocity has a maximum at the center of the tube and gradually falls off to a minimum (near zero) at the walls. Thus, in laboratory flow tubes, it is preferable to maintain turbulent conditions since they are closer to the plug flow conditions (Ref 28:109).

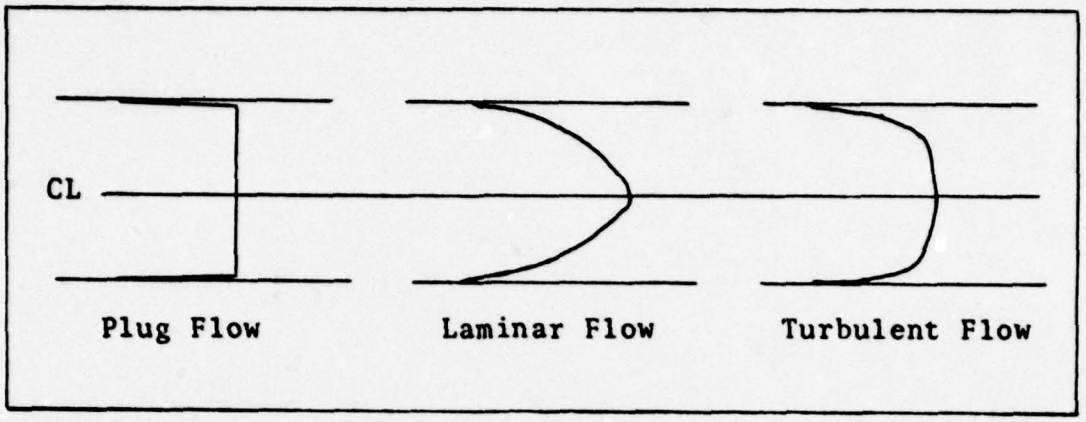

Figure 1. Velocity Profiles

Diffusion can also cause further deviations from plug flow conditions. Diffusion can be defined as the transport of a fluid component under the influence of a concentration gradient by any mechanism of transport. Thus, the rate of transport is given by

$$r = D' \frac{\partial c}{\partial x} \qquad (2\text{-}2)$$

where r is the rate of transport, D' the diffusion coefficient, and $\partial c/\partial x$ the concentration gradient in the x-direction. Transverse diffusion reduces variations of concentration over a cross-section and tends to bring the performance of the flow tube closer to plug flow conditions. That is, transverse diffusion reduces the influence of velocity gradients to normal to the direction of flow. In contrast, longitudinal concentration gradients are such that the diffusional processes tend to carry the fluid toward the

reactor outlet more rapidly than would correspond to the rate of bulk flow.

Large pressure drops in flow tubes also cause deviations from plug flow. The reason for this is, when the flow is very fast, the pressure drop may not be negligible (Ref 20:11-13). For simple Poiseuille flow, the value of this pressure drop can be calculated according to Eq (2-3) (see Appendix B for a derivation).

$$P_2^2 - P_1^2 = \frac{16FL\ R_o\ T\eta}{R^4\ \pi} \qquad (2\text{-}3)$$

where P is the pressure, F the mass flow rate, L and R the length and radius of the tube, η the viscosity, R_o the gas constant, and T the temperature. Thus, large pressure drops violate one of the conditions of plug flow, namely a constant density throughout the flow. It therefore appears that slow flows are desirable because of their negligible pressure drop and rapid radial diffusion. But slow flows may create large axial concentration gradients and increase back diffusion. Therefore, it is necessary to choose a flow rate that minimizes the undesirable effects of both slow flows and very fast flows.

Reattached Flow

To obtain a uniform electric discharge in a flow tube, it is necessary to achieve a reattached flow before the gas reaches the electrodes. This becomes necessary when the

gas line diameter is different than the flow tube diameter. That is, when gas is suddenly expanded as it enters the flow tube, a jet stream develops. Therefore, it is necessary to find a distance downstream from the inlet hole where the flow becomes reattached. Once this distance is determined, the flow tube can be constructed such that the electrodes are immersed in a flow that fills the flow tube cavity.

The effects of suddenly expanding a gas flow were studied by Pennucci (Ref 19:11-15, 20). It was shown in this study that a vortex phenomenon was observed when flows are suddenly expanded, resulting in a recirculation zone (Fig. 2). As the gas enters a suddenly expanded chamber of length L and diameter D, the flow gradually expands until it fills the chamber and becomes reattached. The region at which this occurs is called the attachment region. The point at which the flow becomes reattached is measured from the inlet hole to the center of the attachment region. This distance is known as the recirculation zone length, L'.

Pennucci discovered that the recirculation zone length is a function of the step height parameter. The step height parameter, h, is equal to the difference between the chamber radius and the inlet radius. In flow tube applications, the inlet radius corresponds to the radius of the gas line, and the chamber radius corresponds to the flow tube

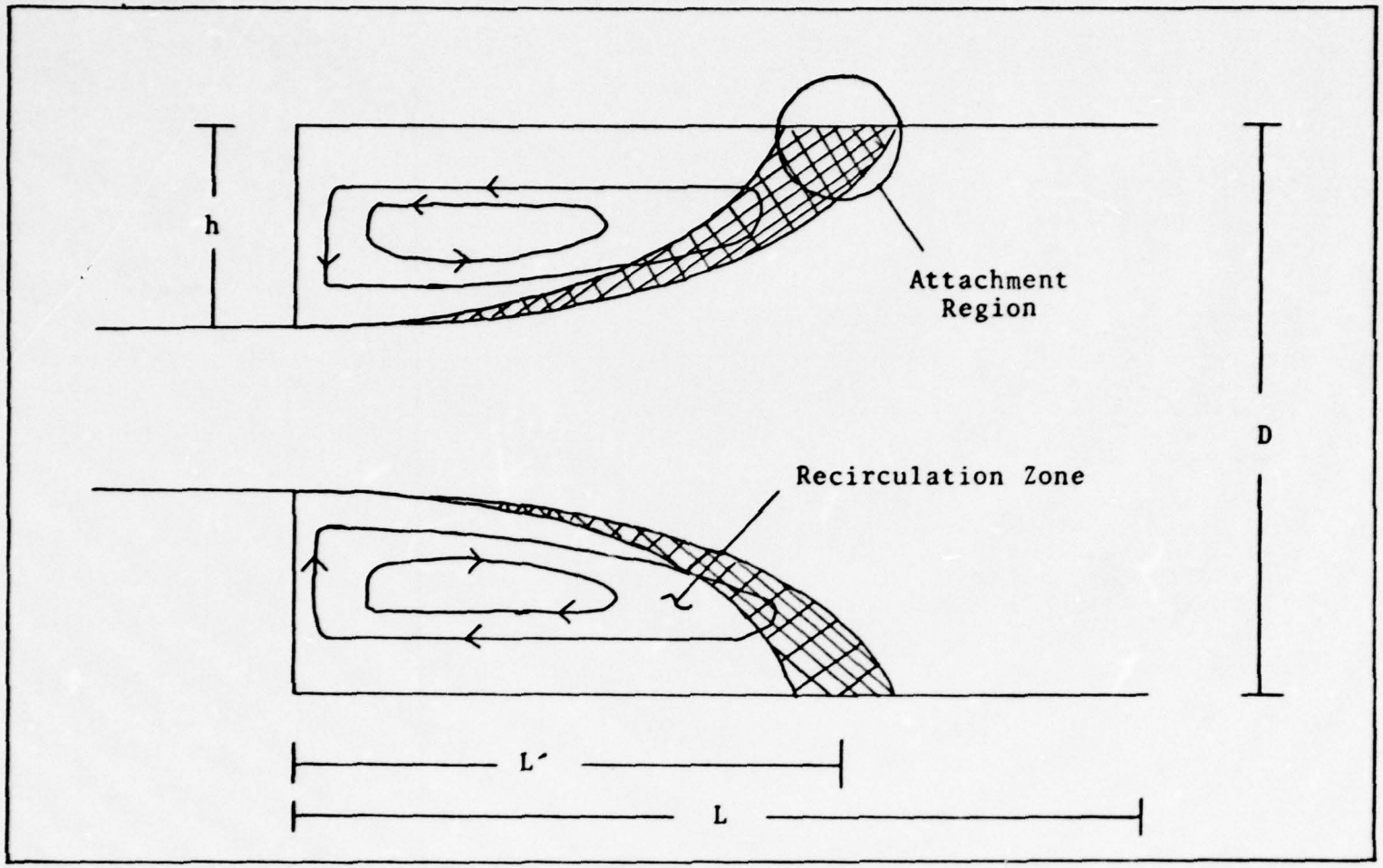

Figure 2. Sudden Expansion Chamber Showing the Recirculation Zone and Flow Reattachment. (Ref 19:30)

radius. Thus, once the step height parameter is calculated, the recirculation zone length, L', is determined by referring to Figure 3. When a flow tube is constructed such that the distance from the inlet hole to the electrodes is greater than L', a reattached flow results before the gas reaches the electrodes. This reattached flow insures a uniform discharge along the flow tube centerline where the electric arc is present. Furthermore, a velocity profile characteristic of the flow conditions begins to form at the reattachment point. Knowing the shape of the velocity profile is an important item in the analysis of a gas flow in a tubular flow reactor.

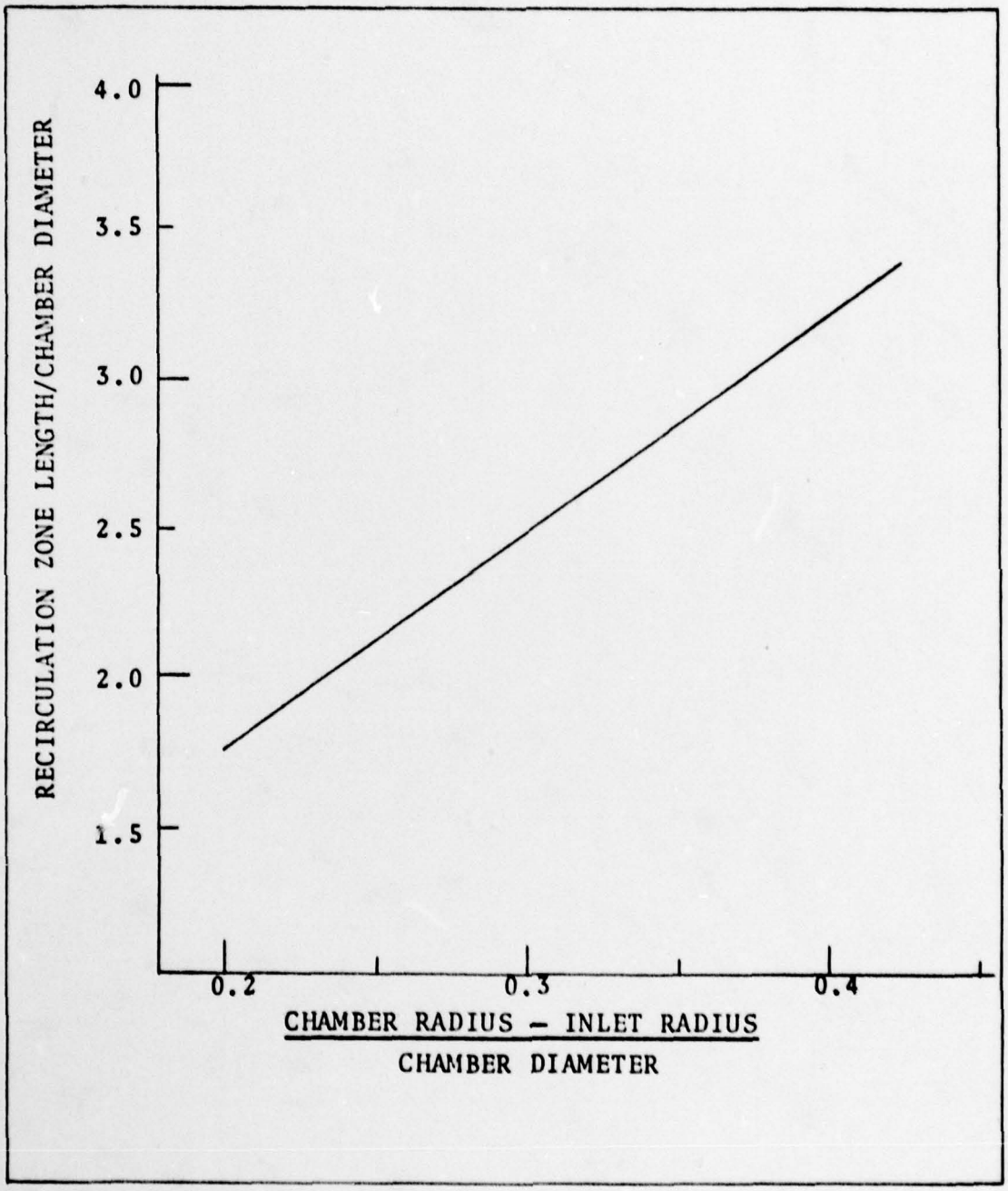

Figure 3. Non-Dimensional Recirculation Zone Length Correlation with Sudden Expansion Step Height. (Ref 19:37)

III. Experimental Apparatus

Introduction

The linear flow velocity and velocity profile of argon was obtained using a fast-flow reactor (flow tube) system. The purpose of this section is to describe the apparatus and arrangement used in this study. To simplify this description, this section is divided into four parts. First, a general description of the flow tube system is given, followed by a description of the three functional parts. These parts include: (1) the gas flow and discharge system, (2) the observation and measurement system, and (3) the pressure measurement and vacuum system.

General

The flow tube arrangement utilized in this experiment was based on the system described by Swearengen (Ref 26:47-48). A few changes were made in the design to meet the requirements of this experiment. The flow tube itself was 162 cm in length and was composed of five sections of pyrex glass tubing. This glass tubing had an inner diameter of 5.1 cm and served to contain the flow of gas. The flow tube was supported by an aluminum stand 25 cm high and 91 cm long. A schematic diagram of the flow tube system is shown in Figure 4. Also, pictures of the flow tube system are presented in Appendix C.

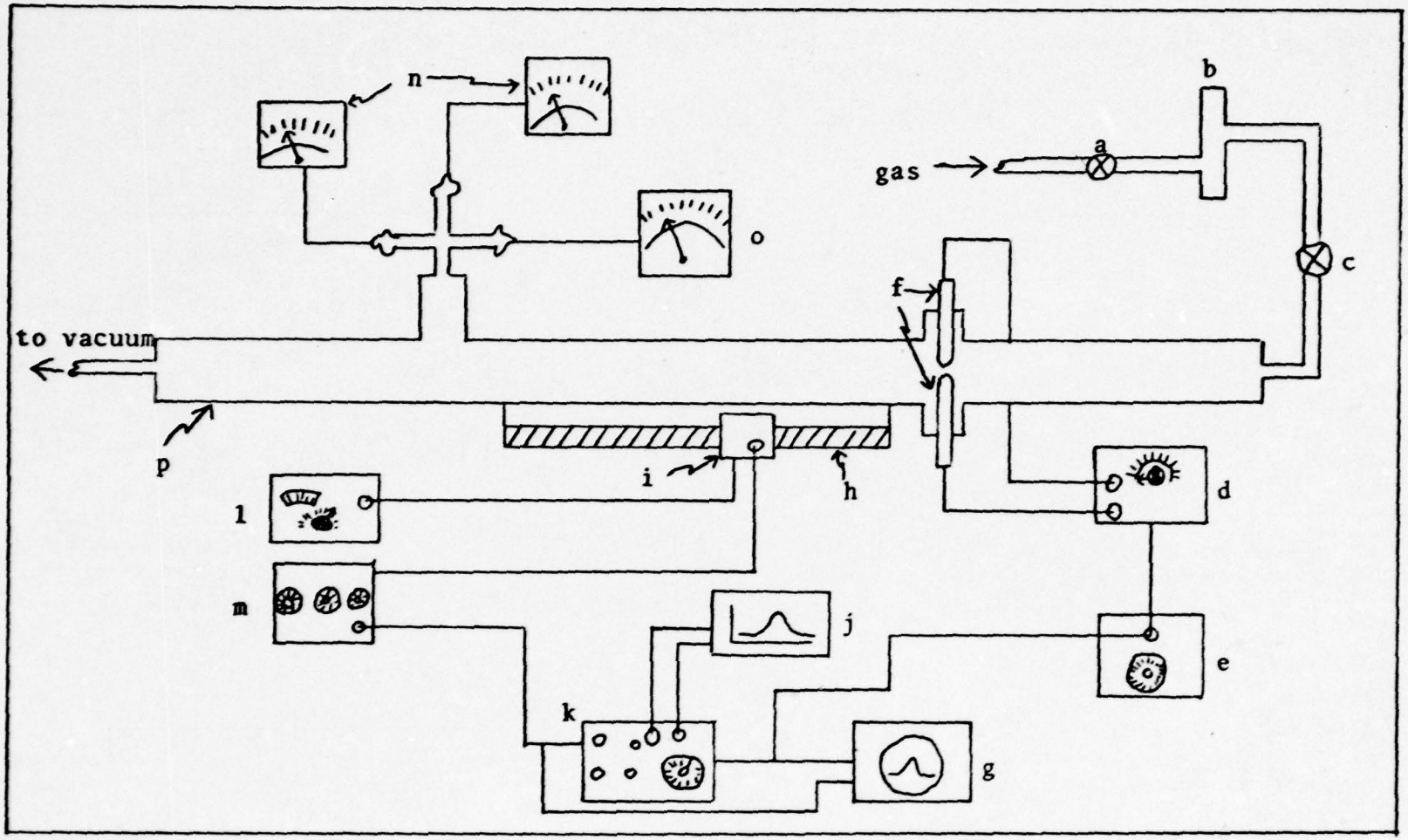

Figure 4. Schematic Diagram of the Experimental Apparatus
(See notation on next page)

Figure 4 Notation. The letters in Figure 4 represent the apparatus used in this experiment. The specific apparatus associated with each letter is listed below.

a. needle valve
b. flowmeter
c. ball valve
d. trigger module
e. square wave generator
f. electrodes
g. oscilloscope
h. optical bench
i. photomultiplier tube (PMT) system
j. x-y recorder
k. signal averager
l. PMT power supply
m. amplifier
n. vacuum guages
o. capacitance manometer pressure gauge
p. flow tube

Gas Flow and Discharge System

The gas flow system furnished the flow tube with a continuous supply of gas. This system included a reservoir of high purity gas, a mass flowmeter, a ball valve, a gas injection tube, and vacuum hose. The vacuum hose had an inner diameter of 1.3 cm and the gas used in this experiment was Matheson high purity grade argon.

A volumetric flow rate was required to calculate the theoretical linear velocity of argon. This flow rate was measured using a Hastings Model A11-10K Linear Mass Flowmeter. The flowmeter was placed 45 cm downstream from the gas tank. A Jamesbury ball valve controlled this flow rate and was placed 15 cm downstream from the flowmeter.

Positioned 120 cm downstream from the ball valve was the gas injection tube, which was the first of the five pyrex

glass tubes making up the flow reactor. This tube was used to obtain a uniform gas flow before the gas reached the electrodes. Therefore, the length of the gas injection tube was determined by the recirculation zone length (Section II, Part 3). Since the inner diameter of the inlet hole and the flow tube was 1.3 cm and 5.1 cm, respectively, the recirculation zone length was found to be 15 cm. This length was determined by referring to Figure 3. Thus, a gas injection tube, 31 cm in length, was chosen for this experiment. The extra length of this tube also aided in the development of the flow profile.

Once this uniform flow was achieved, the gas entered the discharge region. The discharge apparatus initiated the afterglow conditions needed to determine the linear velocity of argon. This apparatus was constructed with a pyrex glass cross, 20 cm in length. The cross was connected to the glass injection tube. The vertical arms of the cross were cylindrical in shape with a 2.5 cm inner diameter. Copper electrodes, .32 cm in diameter, were inserted in these arms through 1.3 cm thick plexiglass plates. A diagram of this apparatus is shown in Figure 5. The electrodes were positioned 40.5 cm downstream from the inlet hole and were adjusted to give a 1 cm gap along the flow tube centerline.

The copper electrodes were connected to an EGG Model TM-11 30 kv trigger module. The trigger module supplied the high voltage necessary to excite the gas. Furthermore,

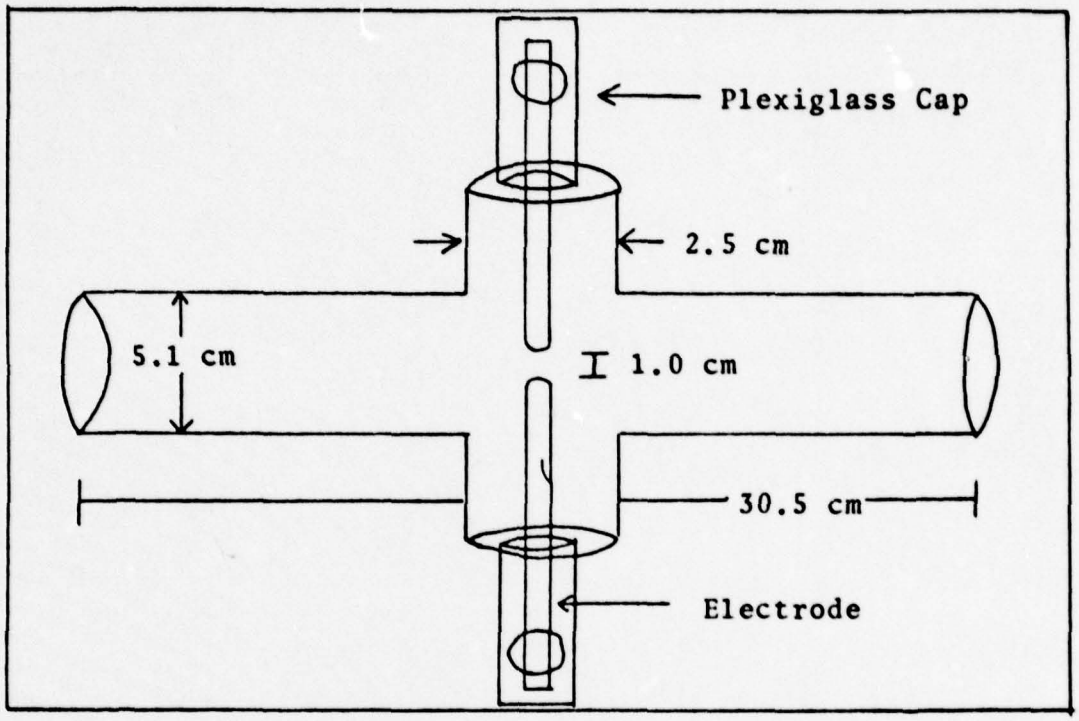

Figure 5. Electric Discharge Section

a repetitive, pulsed discharge was required to produce individual packets of excited gas. The repetitive, pulsed discharge was achieved by triggering the trigger module with a 2 hertz, 20 v peak-to-peak square wave. The square wave was supplied by a Wavetek Model III Voltage Controlled Generator (VCG).

The plexiglass plates which secured the copper electrodes also insulated the electrodes from ground. Plexiglass caps were placed over the electrodes to protect any observers from the high voltage across the electrodes. These caps were 1.3 cm in diameter and 12.5 cm in height.

Observation and Measurement System

The observation and measurement apparatus provided the means to obtain the distance and time measurements required for the velocity calculations. A pyrex glass tube, 61 cm in length, was connected to the cross and used as the observation chamber. A 100 cm long optical bench was positioned alongside this tube. The bench contained a scale to measure distances from the electrodes to the observation point.

A photomultiplier tube (PMT) system, needed to detect the afterglow radiation, was mounted on the optical bench. This system consisted of a 1P21 photomultiplier tube, a variable slit, and a variable iris. The 1P21 photomultiplier tube was chosen for this experiment because of its good response in the visible part of the spectrum. The photomultiplier tube was biased with 1000 volts, supplied by a Furst Model 710-PR HV Power Supply. The variable slit, adjusted to give a width of .2 cm, was placed in front of the photomultiplier tube. The slit allowed a small portion of the radiation from the afterglow to pass to the photomultiplier tube. The iris, adjusted to give a diameter of 1 cm, was placed in front of the slit. The iris allowed the photomultiplier tube to sample the radiation at different heights in the flow.

The output of the photomultiplier tube was fed into a Keithley Model 427 Current Amplifier. This amplified signal was recorded in two ways. First, the signal was sent into a

Princeton Applied Research Model TDH-9 Waveform Educator (signal averager). The Waveform Educator is a device which averages approximately 100 shots or signals that are received by the photomultiplier tube. The signal averager was triggered using the square wave generator that triggered the trigger module. Therefore, the signal averager accepted signals only when the discharge was triggered. The averaged signal was then sent into a Hewlett-Packard Model 7045a X-Y Recorder. Thus, the signal was displayed on a graph of intensity vs time of the averaged signal.

The amplified signals were also recorded photographically. The signals from the amplifier were fed into a Tektronix Model 551 Dual-Beam Oscilloscope which was externally triggered using the Wavetek VCG. These signals were then recorded on Polaroid Type 42 Land Film. Examples of these pictures are displayed in Appendix D.

Pressure Measurement and Vacuum System

Following the observation area, there was a 20 cm long pyrex glass tee. This tee housed the three pressure detection devices which measured the vacuum and the gas pressure in the flow tube. The vertical arm of this tee was cylindrical in shape and had a diameter of 5.1 cm. An aluminum end plate, 1 cm thick, was fastened to this vertical arm. A four-way, female copper fitting, fastened to the end plate, connected the pressure gauges to the flow system. This connection was positioned 122 cm downstream from the inlet hole.

Hastings DV-4D and DV-6 vacuum gauges were used to measure the vacuum in the flow tube. That is, these thermocouple devices measured the pressure in the flow tube with no gas flow. The third pressure measurement device was an MKS Baratron Type 77 Pressure Meter. This capacitance manometer device measured the gas pressure in the flow tube.

The vacuum system, which followed the pressure measurement area, provided a vacuum for the flow tube and a means to flow the gas. This system consisted of a 31 cm long pyrex glass tube, a ball valve, and two vacuum pumps. The glass tube provided an exit port for the gas flow and was connected to the tee. A 1 cm thick aluminum plate was fastened to the exit end of the tube. A hole, 2.5 cm in diameter, was cut in the center of this plate to pass the gas from the flow tube to the vacuum pumps.

Two Welch 17.7 CFM mechanical vacuum pumps provided the vacuum in the flow tube. A pressure of 50 microns was achieved with no gas flow. A vacuum hose, 2.5 cm in diameter, connected the vacuum pumps with the flow tube. A ball valve used to retard the gas flow was placed between the pumps and the flow tube. The purpose of retarding the flow was to provide higher gas pressures in the flow tube.

IV. Experimental Procedure

Introduction

This section describes the procedure that was followed in this experiment. First, a description of the procedure used to obtain the data for the velocity calculations is presented. This is followed by a description of the procedure used to obtain a velocity profile. Finally, the method used to determine the radiative lifetime of the argon metastable state involved in the afterglow effect is described.

Velocity Measurements

The linear velocity of the flowing argon gas was experimentally determined along the flow tube centerline at various gas pressures and flow rates. The photomultiplier tube (PMT) system was laterally traversed along the optical bench and positioned at various distances downstream from the copper electrodes where the gas was excited. The data were obtained by detecting the argon afterglow at these points with the photomultiplier tube. Furthermore, the variable iris, which was considered the front of the photomultiplier tube system, was positioned 2 cm from the outer flow tube wall. The height of the PMT system was adjusted such that the iris was centered along the flow tube centerline ($y = 0$) . This restricted the data acquisition to the flow tube centerline. The linear velocity of argon was determined for the pressures, flow rates, and distances downstream from the electrodes listed in Table II.

Table II

Velocity Measurement Parameters

x (cm)	p (torr)	$\dot{V}$ (std cc/min)
16.9	4.2	4576.0
	6.0	4576.0
26.9	4.2	4576.0
	5.0	5262.4
	6.0	4576.0
	10.1	5262.4
31.9	5.0	5262.4
	10.1	5262.4
33.9	10.1	5262.4
37.1	4.2	4576.0
	5.0	5262.4
	6.0	4576.0
42.1	5.0	5262.4
47.0	4.2	4576.0
	5.0	5262.4
	6.0	4576.0
52.0	5.0	5262.4
56.9	5.0	5262.4
57.4	4.2	4576.0
	6.0	4576.0

The flow tube centerline was determined experimentally. First, a flow of gas was started at an arbitrary flow rate through the tubular reactor. Then, the PMT system was positioned 25 cm downstream from the electrodes. The discharge was initiated next by turning on the trigger module and adjusting the voltage level until a pulse was observed on the oscilloscope. The pulses at various heights in the flow were observed by traversing the PMT system along the vertical axis of the flow tube. These pulses corresponded to the time of flight of the gas from the electrodes to the observation point. Thus, the centerline was determined by fixing the PMT system at the height which corresponded to the fastest time of flight. This fastest time of flight, in turn, corresponded to the maximum velocity of the gas at the operating pressure. This procedure was not repeated for additional flow rates because no accurate means to record the previous result was available.

The data for the linear velocity calculations were obtained in the following manner. A gas flow was first established at a rate of 4576.0 std cc/min. The flow rate was controlled by adjusting the Jamesbury ball valve downstream from the flow meter. The flow rates also determined the gas pressure in the flow tube, and at 4576.0 std cc/min the gas pressure was 4.2 torr. With the gas flowing, the trigger module was turned on, initiating the spark discharge. The PMT system was then placed at the first station located 16.9 cm downstream from the electrodes. The electrical

pulse which resulted from the detection of the afterglow was observed on the oscilloscope and recorded photographically. After these data were recorded, the PMT system was moved farther downstream from the electrodes. Four additional stations were chosen as observation points (see Table II) and recorded in the same manner as mentioned above. Samples of these pictures are displayed in Appendix D.

Upon completing the data acquisition at 4.2 torr, the gas flow was retarded by closing the ball valve located near the vacuum pumps. This choking process resulted in an increased gas pressure in the flow tube, but no change in the flow rate. A back-pressure of 6.0 torr was chosen for the next set of velocity calculations, and the experiment was repeated at this pressure.

Additional data were obtained for the velocity calculations by changing the flow rate. The Jamesbury ball valve was adjusted such that a gas pressure of 5.0 torr was established in the flow tube. This resulted in a new flow rate of 5262.4 std cc/min. Again, the discharge was initiated by turning on the trigger module. The PMT system was then moved to a location 26.9 cm downstream from the electrodes (station 1). In this part of the experiment, the electrical signal from the current amplifier was sent into the signal averager. This technique reduced the data acquisition time by acquiring a single pulse which was the average of 100 individual pulses. The averaged pulse was observed on the oscilloscope and recorded using the x-y recorder. On the

graph paper, the relative signal intensity, I_R , was plotted against the time, t , it took for the excited gas to reach the observation point. A time scale of 0 - 100 msec was chosen for accurate time determinations. After the signal at station 1 was recorded, the PMT was moved to a new location farther downstream from the electrodes. Six additional locations were chosen as observation points (see Table II), and the data were recorded in the same manner as mentioned above.

Once the data collection at 5.0 torr was completed, the flow was retarded by closing the ball valve located near the vacuum pumps. A gas pressure of 10.1 torr was chosen for this part of the experiment, with a flow rate of 5262.4 std cc/min. The experiment was repeated for these conditions, but only two additional stations were used as observation points.

Velocity Profile Measurement

The velocity profile of the flowing argon in the tubular reactor was determined at 5.0 torr with a flow rate of 5262.4 std cc/min. The PMT system was positioned 28.5 cm downstream from the electrodes with the iris centered on the flow tube centerline. The PMT was then vertically traversed along the flow tube at that position to determine the radial profile of the velocity. The data were recorded at .5, 1, 1.5, and 2 cm above and below the flow tube centerline. This procedure was repeated with the PMT system located 35.9 cm downstream from the electrodes.

Radiative Lifetime Determination

The procedure in this experiment was essentially the same as the procedure followed in the determination of the linear velocity of argon. The gas flow was maintained at a flow rate of 5262.4 std cc/min and a gas pressure of 5.0 torr. After the trigger module was turned on, the PMT system was positioned 24.4 cm downstream from the electrodes along the flow tube centerline. All the electronic equipment was adjusted such that a maximum signal was observed on the oscilloscope at this station. The same settings were maintained on the electronic equipment for the subsequent readings. The purpose of this was to obtain data such that variations in the intensity of the peaks could be observed. Thus, a decay rate could be determined and a Stern-Volmer plot constructed to determine the radiative lifetime (Ref 33:1567).

The PMT was moved to three additional stations downstream from the electrodes after the pulse was recorded on the graph paper at the 24.4 cm location. The location of the additional data collecting stations are listed in Table III. Upon completing the data gathering at 5.0 torr, the gas flow was retarded such that a gas pressure of 7.0 torr was obtained. The settings on the electronic equipment remained constant as set previously. The data at 7.0 torr were recorded at four stations downstream from the electrodes. (See Table III)

Table III

Parameters for Radiative Lifetime Determination

x (cm)	p (torr)
24.4	5.0
	7.0
26.4	7.0
28.2	7.0
33.5	5.0
	7.0
40.4	5.0
42.4	5.0

V. Results and Discussion

Introduction

The experimental and theoretical results of this study are presented in this section. Comparisons are made between these results to determine the validity of the plug flow assumption in flow tube applications. First, the experimental and theoretical (plug flow) velocity calculations are presented. This is followed by a presentation and a discussion of the experimental and theoretical velocity profiles. Then, the validity of the plug flow assumption is determined in Part 4 using the above results. The radiative lifetime of the argon metastable state which produced the afterglow is calculated in Part 5.

Velocity Calculations

The linear velocity of argon was calculated by performing a linear regression on the raw data at 4.2, 5.0, and 6.0 torr. No linear regression was done on the data at 10.1 torr because only four values were recorded. Since it was assumed that no random error was associated with the distance measurements, the linear least squares fit was computed by regressing t on x. A plot of t versus x was constructed with the equation of the line which resulted from the linear regression. At 10.1 torr, the four data points were directly plotted and the best fitted line was drawn

through them. The linear velocity of argon was then determined by inverting the slopes of the lines. The raw data used in the linear least squares fit are tabulated in Appendix E.

All the time measurements were recorded at the point where the pulse began to rise to eliminate the three dimensional effect of the gas flow (Figure 6). That is, the photomultiplier tube detected the afterglow radiation in a one dimensional plane. As the gas passed in front of the PMT system, the radiation emitted from the gas layers in front and in back of the centerline layer was detected. Since the gas velocity of these layers is slower than that at centerline, the recorded pulse did not fully reflect the centerline velocity beyond the point where the pulse began to rise. The result of detecting this slower gas flow lengthened the width of the recorded pulse and made the pulse non-symmetric (Figure 6). Furthermore, the fairly wide field of view of the optical system facilitated the detection of the radiation and was the main cause for the non-symmetric curve. Therefore, the point where the pulse began to rise was the only reliable time measurement for the centerline layer of gas, and corresponded to the maximum velocity (shortest time of flight from the electrodes to the observation point) of the packet of excited gas.

The theoretical or plug flow value of the linear velocity of argon was calculated using Eq (5-1).

$$U_{pf} = \frac{Q \times P(atm) \times 1.43}{60 \times P(gas) \times A} \qquad (5\text{-}1)$$

where Q is the volumetric flow rate of air in standard cc/min, p(atm) the atmospheric pressure in torr, p(gas) the gas pressure in torr, A the cross-sectional area of the flow tube, and 60 the conversion factor from minutes to seconds. To convert the volumetric flow rate of air to that of argon, Q was multiplied by 1.43 ($V = Q \times 1.43$). This conversion factor was obtained from the Hasting Mass Flowmeter literature. The ratio p(atm)/p(gas) converted the volumetric flow rate at standard conditions to that of the operating gas pressure. The temperature was assumed to remain constant throughout the experiment at room temperature since no chemical reactions took place.

The results of the velocity calculations are summarized in Table IV and Figure 7. Table IV lists the linear gas velocities at various pressures. These values were obtained from the inverted slopes of the lines in Figure 7. The correlation coefficients from the linear regression analysis are also included in Table IV. The errors quoted in the linear velocity values are standard deviations in time since no error was associated with the distance measurements. Finally, Table V lists the results obtained from the plug flow calculations.

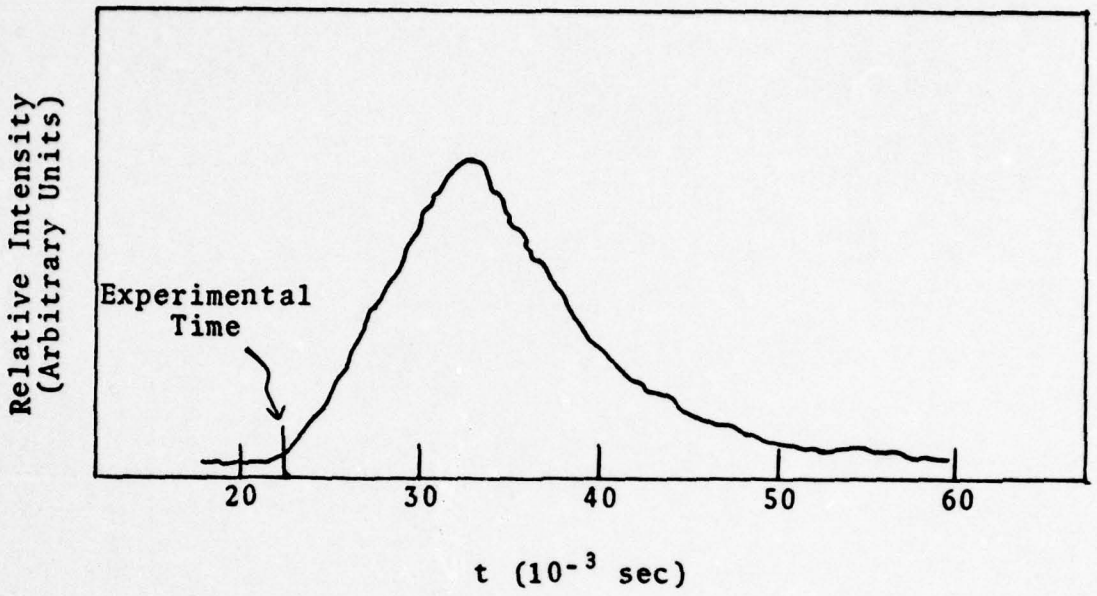

Figure 6. Sample Pulse at 5.0 Torr

Table IV

Experimental Linear Velocities

p (gas)	u_e (cm/sec)	r
4.2	$(1.08 \pm .017) \times 10^3$	.994
5.0	$(1.14 \pm .015) \times 10^3$	.981
6.0	$(7.83 \pm .02) \times 10^2$	.986
10.1	5.51×10^2	----

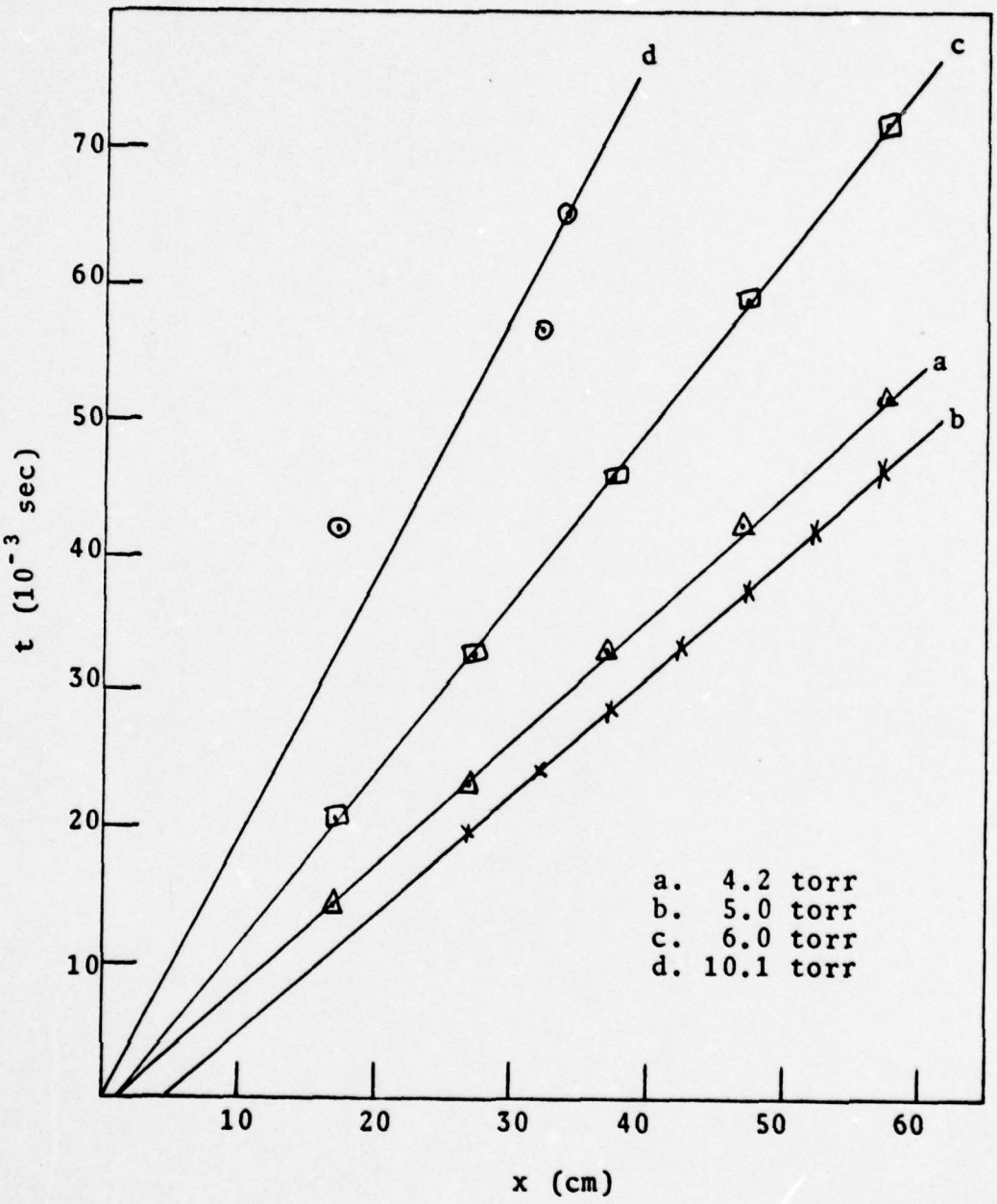

Figure 7. Analysis of Velocity Experiment at Various Pressures

Table V

Plug Flow Velocity Results

p(gas) (torr)	p(atm) (torr)	$\dot{V}$ (std cc/min)	A(cm^2)	u_{pf}(cm/sec)
4.2	740.1	4576.0	20.27	663.01
5.0	736.4	5262.4	20.27	637.27
6.0	740.1	4576.0	20.27	464.65
10.1	736.4	5262.4	20.27	315.48

Velocity Profile Results

The velocity profile of the gas flow was dependent upon the type of flow present (molecular, viscous, or intermediate). The division between these flow regimes was determined by the value of the Knudsen number as stated in Appendix B. In this study, the mean free path of argon at 5.0 torr was calculated to be 1.04×10^{-3} cm . Therefore, the Knudsen number for this gas flow was 4884.6 . Since this value of the Knudsen number is greater than 110 (Appendix B), the flow was viscous. Furthermore, the Reynolds number was 280 which showed that the flow was laminar as well. Therefore, a velocity profile characteristics of a laminar flow was predicted to form in the flow tube.

The instantaneous linear velocity of argon was calculated at various heights above and below the flow tube centerline. The data for these calculations were obtained at 28.5 and 35.9

cm downstream from the electrodes. These experimental velocities were then plotted against distance above and below the flow tube centerline to obtain the profile. The experimental velocity values are listed in Table VI. Figure 8 shows the velocity profile at the two observation points.

The solid parabolic curve in Figure 8 is a theoretical velocity profile characteristic of fully developed internal flows. This profile was determined using Eqs (B-17) and (B-18). That is,

$$u_{AV} = \frac{-R^2}{8\eta} \frac{\Delta P}{\Delta X} \qquad \text{(B-17)}$$

and

$$u = 2\, u_{AV} \left[1 - y^2/R^2\right] \qquad \text{(B-18)}$$

The average velocity of argon at 5.0 torr calculated from Eq (B-17) was 637.6 cm/sec. This value was obtained at both 28.5 and 35.9 cm downstream from the electrodes. The viscosity used in this equation was 223.37×10^{-6} poise with $R = 2.5$ cm .

The experimental velocity profiles shown in Figure 8 resemble the theoretical curve out to $\pm$ 1 cm from the centerline. At distances greater than $\pm$ 1 cm from the centerline, the experimental values deviate from the theoretical curve. This deviation was mainly due to

Table VI

Experimental Linear Velocities at Various Heights Above and Below the Flow Tube Centerline

y (cm)	x (cm)	u_e (cm/sec)
2.0	28.5	1017.9
	35.9	957.3
1.5	28.5	1055.6
	35.9	1104.6
1.0	28.5	1140.0
	35.9	1139.7
0.5	28.5	1127.5
	35.9	1158.1
0.0	28.5	1266.7
	35.9	1305.7
-0.5	28.5	1172.8
	35.9	1158.1
-1.0	28.5	1140.0
	35.9	997.2
-1.5	28.5	1083.7
	35.9	897.5
-2.0	28.5	934.4
	35.9	763.8

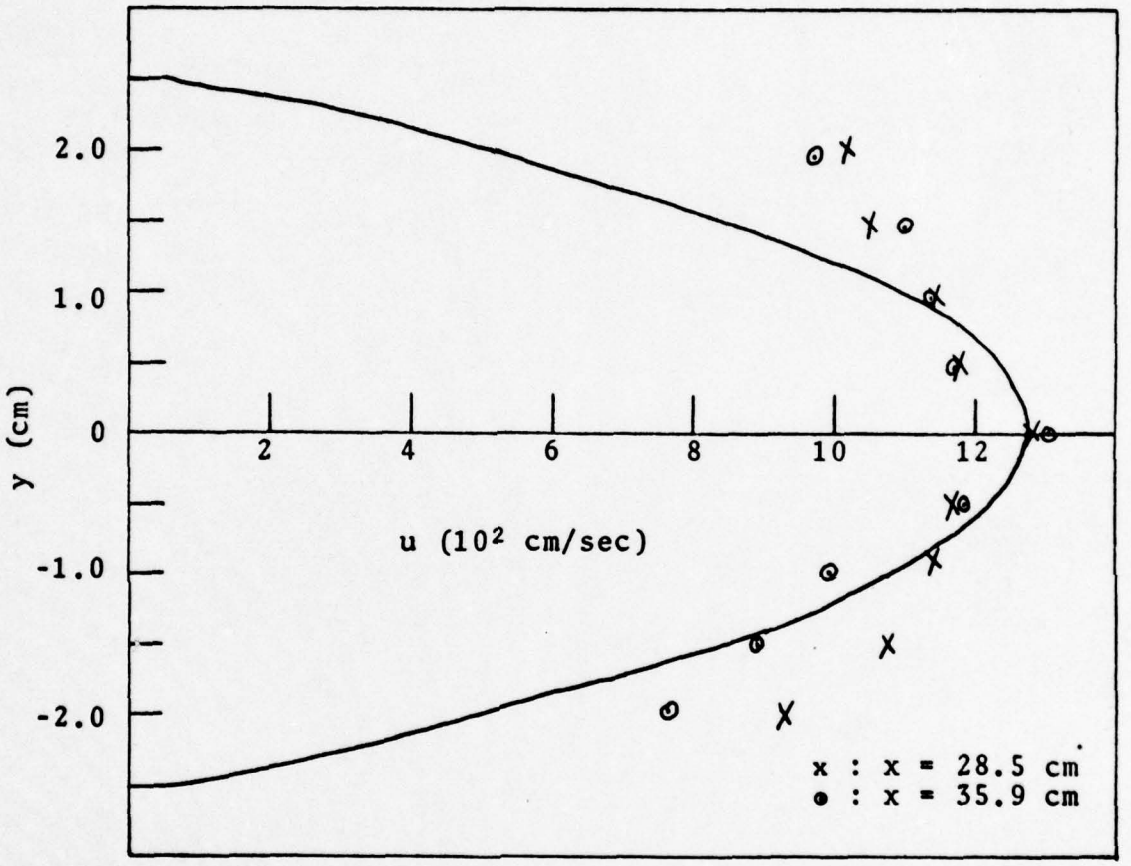

Figure 8. Experimental and Theoretical Velocity Profiles at 5.0 Torr

turbulence around the electrodes. This slight turbulence affected the symmetry of the profile at points near the upper and lower flow tube walls. Furthermore, the curvature of the glass tube became more pronounced at these points. The increased curvature of the tube, coupled with the fairly wide field of view of the optical system, focused unwanted

radiation from slightly lower gas layers onto the PMT system. Therefore, the velocities obtained from these data curves were faster than expected.

Since both profiles were parabolic within experimental scatter, the flow was considered fully developed at 28.5 cm downstream from the electrodes. The characteristic length for an internal flow to become fully developed was calculated using Eq (5-3).

$$X_L = .03 \text{ (Re) } D \qquad (5\text{-}3)$$

where X_L is the laminar development length, Re the Reynolds number, and D the tube diameter. The laminar development length was calculated as 42.67 cm from the point where the flow became reattached at the inlet section (Figure 2). Therefore, the flow was fully developed 16.67 cm downstream from the electrodes.

These results were confirmed with similar calculations performed by Rapagnani and Davis (Ref 20). The distance and time measurements of some representative pulses obtained in this study at 5.0 torr were written into a computer program. This program calculated linear velocities of gases at various normalized distances from the flow tube centerline. This axi-flow tube velocity calculation of 100% argon at 5.0 torr was utilized for a flow tube of radius 2.959 cm. The results of the program are displayed in Figures 9 through 12.

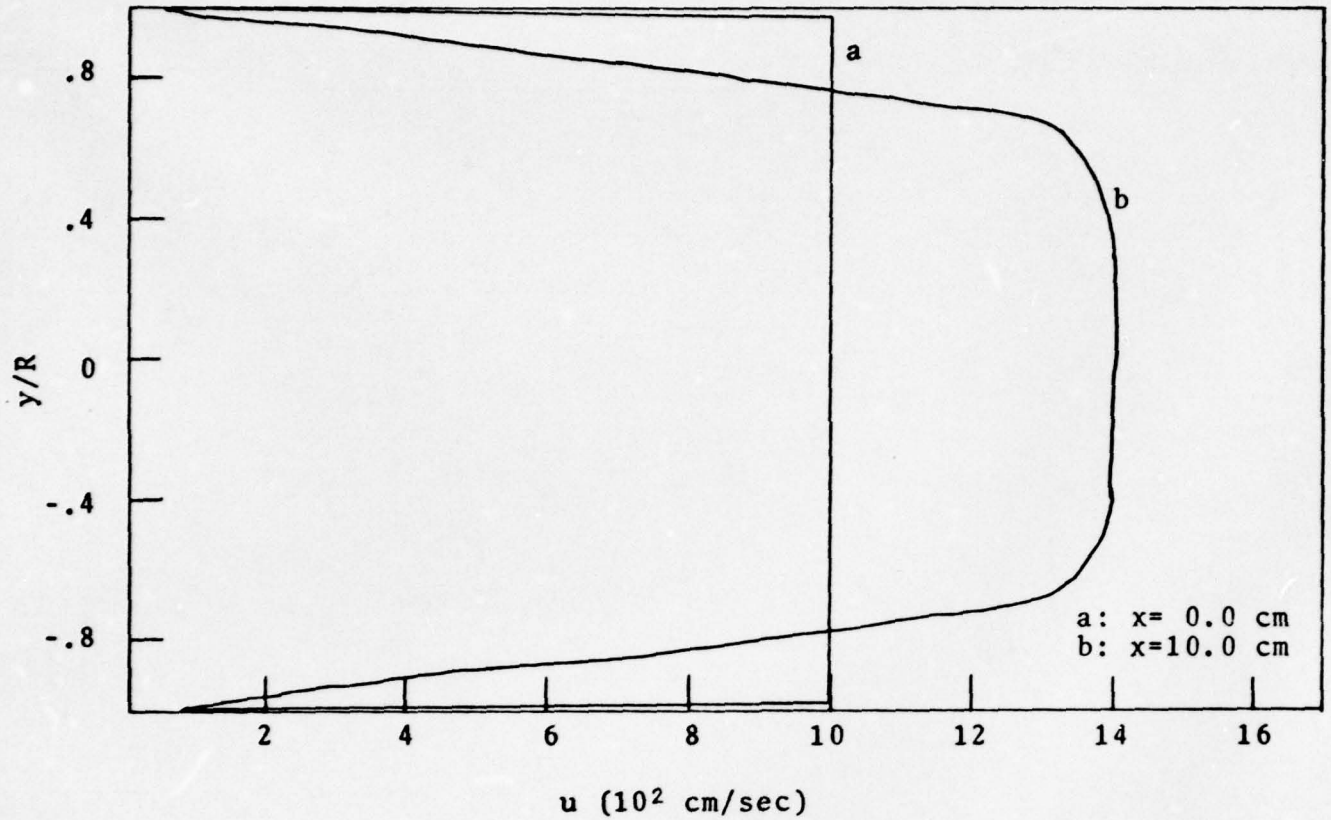

Figure 9. Velocity Profile for a Flow Tube with with R = 2.959 cm at x = 0.0 cm and x = 10.0 cm.

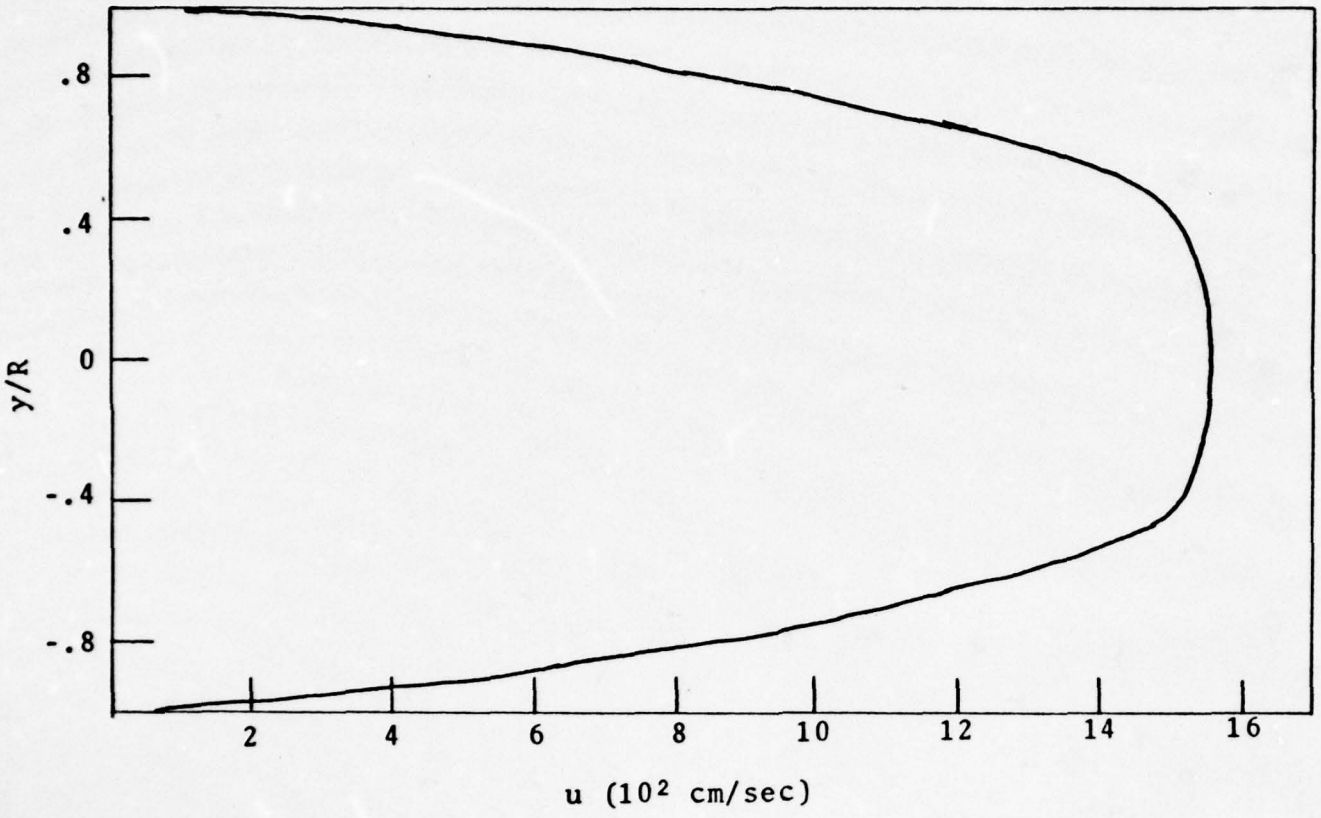

Figure 10. Velocity Profile for a Flow Tube with R = 2.959 cm at x = 20.0 cm

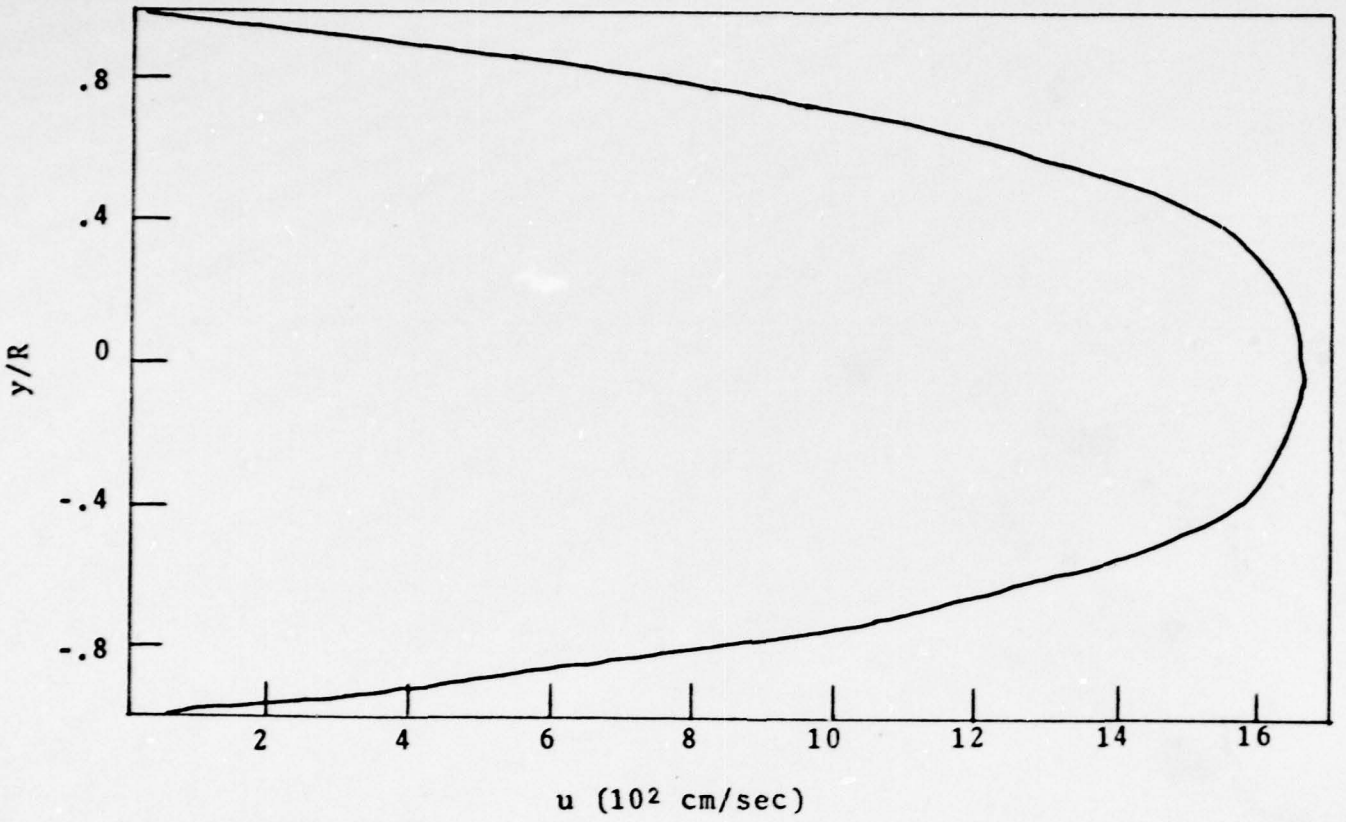

Figure 11. Velocity Profile for a Flow Tube with R = 2.959 cm at x = 30.0 cm

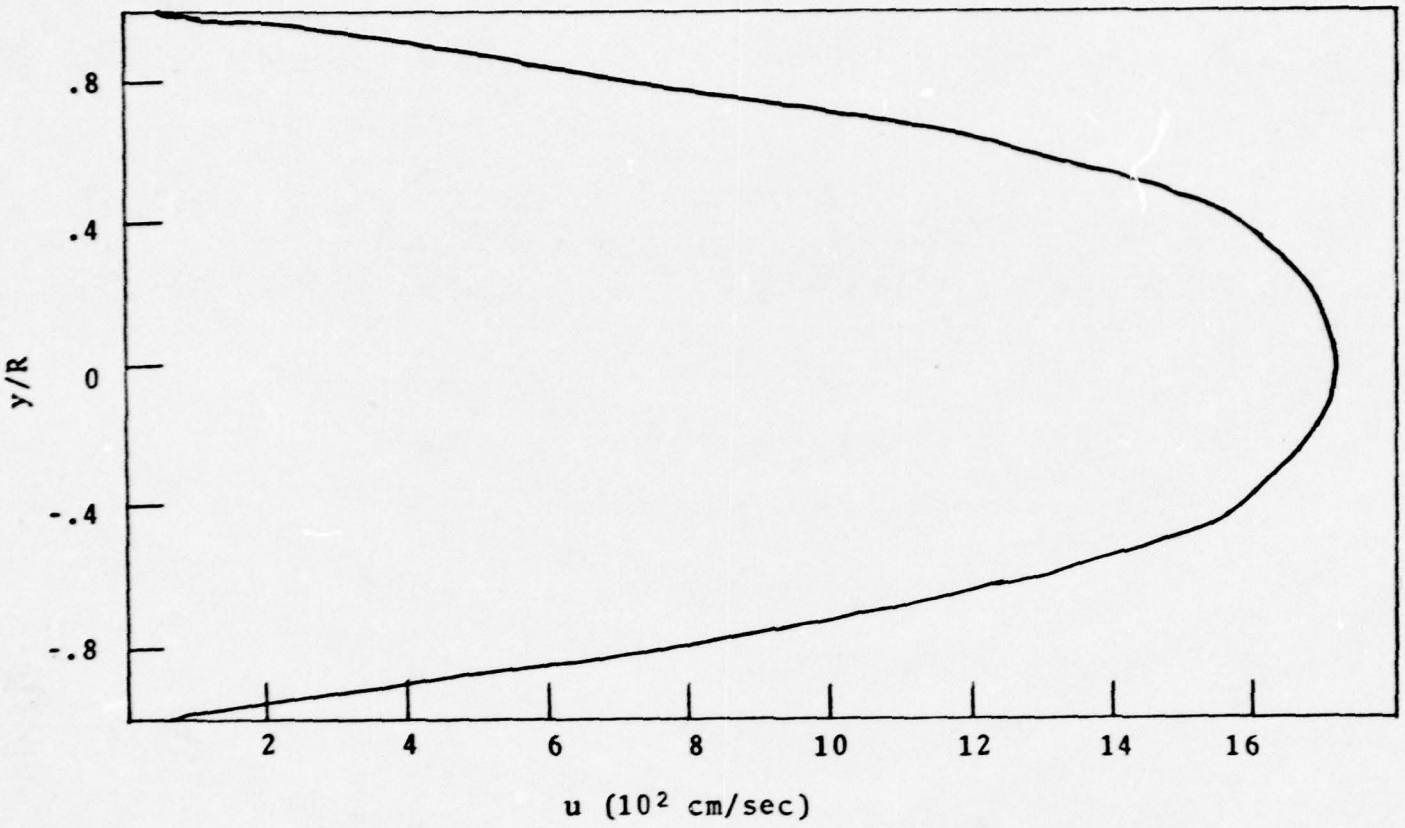

Figure 12. Velocity Profile for a Flow Tube with R = 2.959 cm at x = 40.0 cm

The velocity profile at 10 cm downstream from the electrodes (Figure 9) had a flat head for a distance ± .4 cm from the centerline. This configuration was characteristic of a developing internal flow. The profile approached a parabolic configuration at $x = 20$ cm (Figure 10). But, a fully developed flow, characterized by a parabolic velocity profile, was not observed until the flow was 30 cm downstream from the electrodes (Figure 11). The flow was considered fully developed at $x = 30$ cm because the profile did not change farther downstream from the electrodes (Figure 12). Therefore, the point where the flow became fully developed was located between $x = 20$ cm and $x = 30$ cm . Furthermore, for a flow tube 2.959 cm in radius, the laminar development length, X_L , was 49.7 cm downstream from the flow reattachment point (Figure 2). The point where the flow became fully developed was then calculated as 23.7 cm downstream from the electrodes since the distance between the electrodes and the reattachment point was 26.0 cm.

Since the laminar development length, X_L , calculated from the computer results comparatively agreed with the experimental results at 5.0 torr, the laminar development length was calculated for the other operating pressures. Table VII lists the values of X_L for 4.2, 6.0, and 10.0 torr. The value of X_L in this table is a distance downstream from the electrodes. The corresponding Knudsen and Reynold numbers are also listed in the table.

Table VII

Flow Regimes and Laminar Development Lengths for Gas Pressures fo 4.2, 6.0, and 10.1 Torr

p (torr)	λ(cm)	η(10^{-6} poise)	Kn	Re	Flow Regime	X_L (cm)
4.2	1.25×10^{-3}	224.21	4064	222.4	viscous laminar	7.89
6.0	8.7×10^{-4}	223.73	226.3	230.4	viscous laminar	9.1
10.1	5.16×10^{-4}	223.37	984.5	297.4	viscous laminar	19.32

It was noticed in Table VII that X_L increased as pressure increased for a constant flow rate. This trend was attributed to decreasing pressure losses in the flow tube. Since pressure losses occur in internal flows as a result of friction, an increased gas pressure also resulted in decreased frictional losses. The relationship between the pressure drop and the friction factor is given in Eq (5-4).

$$\frac{\Delta p}{\rho g} = \left(\frac{L}{D}\right) \frac{u_{av}^2}{2g} f = H_L \qquad (5\text{-}4)$$

where Δp is the pressure change, ρ the density, g the acceleration due to gravity, L and D the length and diameter of the tube, respectively, u_{av} the average

velocity, f the friction factor, and H_L the head loss. The friction factor for laminar flow is determined by

$$f = 64/Re \qquad (5\text{-}5)$$

Therefore, an increased gas pressure resulted in an increased Reynolds number and a decreased friction factor. This decreased friction factor then reduced head loss or pressure loss. An increased Reynolds number also increased the laminar development length as given by Eq (5-3).

Plug Flow Validity

The velocity profiles of argon at various pressures were parabloic within the experimental scatter which suggested that a fully developed laminar flow was present throughout the experiment. An interesting relationship existed between the plug flow velocities and the average velocities calculated using Eq (B-17). As mentioned in Section II, Part 3, the plug flow calculations gave the average velocity of the gas flow. The values of the plug flow velocity and the calculated average velocity are compared in Table VIII. The results of Table VIII show that the plug flow velocities are equal to the average flow velocities. Thus, the plug flow velocity can be used as the average velocity in flow calculations.

The results of the linear velocity calculations along the flow tube centerline should be twice the average or plug

flow velocity. This is evident when $y = 0$ in Eq (B-18). A comparison between the linear velocity results at $y = 0$ and the plug flow values are given in Table IX. The results show a discrepancy between the experimental and theoretical results. This discrepancy is possibly due to the turbulence from the electrodes which would tend to reduce the ratio u_e / u_{pf}. Furthermore, the hollow arms of the cross, which was used to house the electrodes, added two cavities to the inner flow tube wall. These cavities further distorted the flow profile and possibly affected the gas flow along the centerline. Therefore, the ratio u_e / u_{pf} would further decrease.

Another trend is seen in the velocities listed in Table IX. At a constant flow rate, the velocities decrease linearly with increasing pressure. For example, the velocity at 5.0 torr is approximately two times the velocity at 10.0 torr. This result held true for both the experimental and plug flow velocity values.

It was mentioned in Section II, Part 2, that four conditions tended to bring the flow away from plug flow. These conditions were (1) large temperature gradients, (2) large velocity gradients normal to the flow direction, (3) a large pressure drop, and (4) large longitudinal diffusion. In this study, large temperature gradients did not exist since chemical reactions were absent. On the other hand, the velocity profiles were parabolic which suggested that large velocity gradients were present.

Table VIII

Plug Flow and Average Velocities

p (torr)	u_{av} (cm/sec)	u_{pf} (cm/sec)
4.2	664.78	663.01
5.0	638.72	637.27
6.0	465.32	464.65
10.1	315.67	315.48

Table IX

Comparison of Experimental and Plug Flow Velocities

p (torr)	u_e (cm/sec)	u_{pf} (cm/sec)	u_e/u_{pf}
4.2	1085.27 ± 16.7	663.01	1.64
5.0	1138.53 ± 15	637.27	1.79
6.0	738.27 ± 20.3	464.65	1.59
10.1	551.12	315.48	1.75

Table X

Calculated Pressure Changes
Experienced by Argon at Various Pressures

p (torr)	Δp (torr)
4.2	2.246×10^{-2}
5.0	2.15×10^{-2}
6.0	1.57×10^{-2}
10.1	1.063×10^{-2}

Therefore, plug flow was not achieved in the experiment.

Large pressure drops cause deviations from plug flow by producing a density gradient normal to the direction of flow. In this study, the pressure drop at all the operating gas pressures was not negligible (see Table X). Therefore, a rapid radial diffusion was not present to minimize the density gradient. A longitudinal diffusion problem does not exist in a flow tube operating in a laminar flow regime. This is evident by considering Eq (5-6).

$$D_{11} = (6/5)\, \eta/\rho \qquad (5\text{-}6)$$

where D_{11} is the self-diffusion coefficient, η the viscosity, and ρ the density. At higher pressures, the density becomes larger, thereby reducing D_{11} . In

molecular flow regimes where the pressure is on the order of 10^{-6} torr, the self-diffusion coefficient becomes large and longitudinal diffusion brings about a deviation from plug flow. In this study, the pressures were in the laminar flow range, which resulted in negligible longitudinal diffusion.

Radiative Lifetime Determination

The radiative lifetime of the argon metastable state responsible for the afterglow was determined in this experiment. First, decay rates were calculated for argon at 5.0 and 7.0 torr. Then, these decay rates were plotted versus total gas pressure to obtain a Stern-Volmer plot. The y-intercept of the line on the Stern-Volmer plot, the decay rate $(1/\tau)$ axis, determined the value of the radiative lifetime.

The decay rates were obtained by first measuring the heights of the recorded pulses. The vertical axis of the graph, which plotted the intensity of the pulse, was labeled from one to ten with each increment ten squares apart. Thus, the relative intensity, I , of each pulse was noted by measuring the height of the pulse at its peak relative to the y-axis scale. These relative intensities were then normalized with respect to the most intense pulse at each pressure. That is, all the relative intensities of the pulses at 5.0 torr were normalized with respect to the most intense pulse at 5.0 torr obtained at the station closest to the electrodes.

Table XI

Data for Lifetime Determination

p (torr)	x (cm)	t (msec)	I	I_n	$1-I_n$
5.0	24.4	26.0	7.55	1	0
	33.5	37.5	3.80	.503	.497
	40.4	41.3	2.50	.331	.669
	48.4	44.0	0.99	.131	.869
7.0	24.4	36.5	2.7	1	0
	28.2	40.8	2.25	.833	.167
	33.5	46.0	0.85	.315	.315

The relative intensities of the pulses were proportional to the number of excited states present at that time and location. Therefore, all the normalized intensities, I_n , were subtracted from one to give a quantity which was proporational to the number of states that had decayed. This quantity, $(1-I_n)$, was plotted versus time, and the slopes of the lines on the graph revealed the decay rate of argon at a particular pressure. Table XI lists the relative intensities, normalized relative intensities, and the quantity $(1-I_n)$ for this experiment. The quantity $(1-I_n)$ is plotted versus time in Figure 13. It was determined from this graph that the decay rate of argon at 5.0 torr was 46.7 sec^{-1} and at 7.0 torr, $1/\tau = 63.7\ sec^{-1}$.

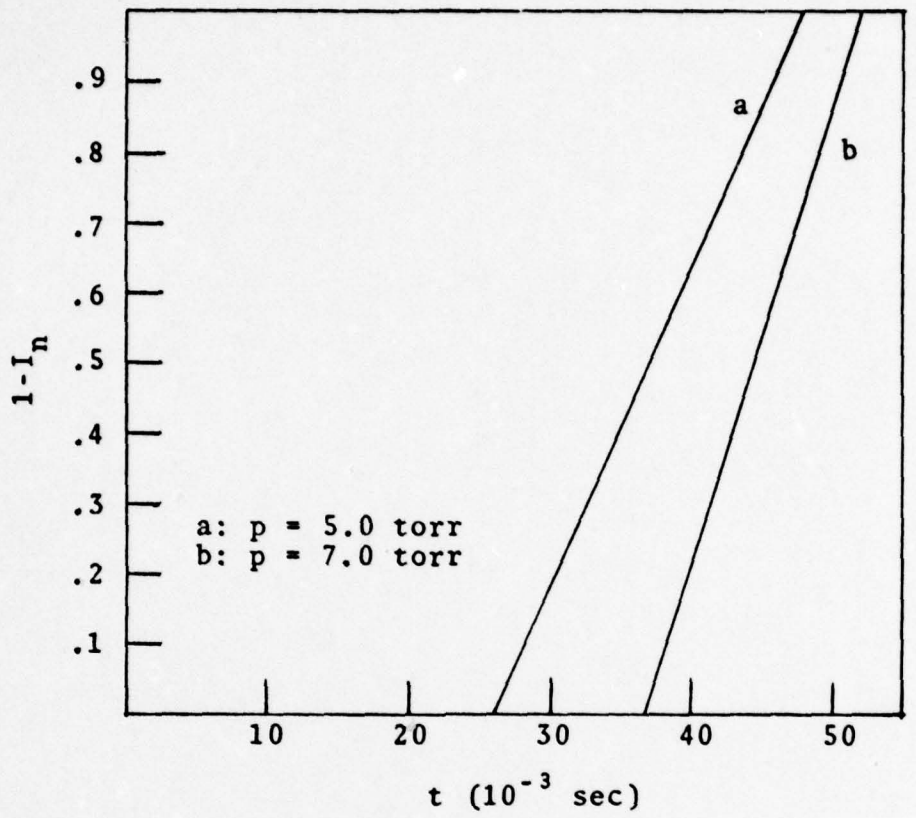

Figure 13. Decay Rate of Argon at 5.0 and 7.0 Torr

The decay rates were plotted against total gas pressure to obtain a Stern-Volmer plot (Figure 14). The transition probability of this metastable state was determined from the y-intercept of the plotted line. The transition probability for the argon metastable state responsible for the afterglow in this experiment was 0.4 sec^{-1} . This transition probability corresponded to a radiative lifetime of 250 msec. As explained in Section II, Part 2, the radiative lifetime of the metastable state had to be at least the same order as the time of flight from the electrodes to the observation

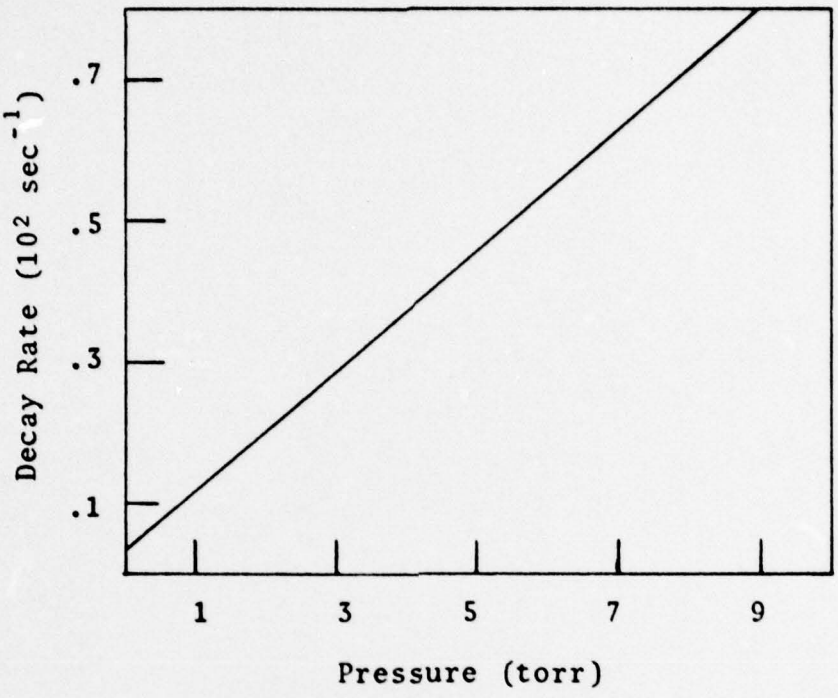

Figure 14. Stern-Volmer Plot of Decay Rate Versus Total Gas Pressure for Argon

point to detect the afterglow. A lifetime of 250 msec easily fulfilled this requirement.

It was determined that the particular transition which produced the afterglow was either the $^1P - {}^1S$ multiplet of Ar III or the $^1D - {}^1S$ multiplet of Ar V (Ref 31:214, 217). The $^1P - {}^1S$ multiplet of Ar III has a transition probability of 4.02 sec^{-1} and radiated at 3109 Å. On the other hand, the $^1D - {}^1S$ multiplet of Ar V had a transition probability of 3.8 sec^{-1} with an emitted wavelength of 4625.54 Å. Since the 1P21 PMT had excellent response characteristics in the visible part of the spectrum and a very poor response in the uv, the $^1P - {}^1S$ multiplet of Ar III was ruled out as the

appropriate transition. Therefore, it was suggested by this study that the ^1D - ^1S multiplet of Ar V was responsible for the afterglow. Additional data are required for a more accurate determination of this metastable state.

It was observed that the decay rate was attributed to the increase in the number of collisions in the flow tube (Appendix F). In other words, as the pressure increased, the mean free path between atoms was reduced, which resulted in a larger collision rate. For example, the mean free path and collision rate of argon at 5.0 torr were 1.04×10^{-3} cm and 3.8×10^{7} sec^{-1}, respectively. At 10.1 torr, these quantities became 5.16×10^{-4} cm and 7.7×10^{7} sec^{-1}, respectively. These results are summarized in Table XII. In Table XII, σ is the collision diameter, η the viscosity, $\langle u \rangle$ the average Maxwellian velocity, N* the number of atoms per unit volume, λ the mean free path, and z the number of collisions per second.

Furthermore, the effectiveness of collisional de-excitation was determined with the aid of the collision rates. The number of atoms that have not undergone a collision was calculated using Eq (5-7) (Ref 17:101).

$$N = N_0 e^{-zt} \tag{5-7}$$

where N_0 is the number of atoms at $t = 0$ and z the collision rate. At the lowest operating pressure in this

Table XII

Collision Parameters at Various Gas Pressures

p(torr)	T(°K)	$\eta(10^{-6}$ poise)	$\sigma(10^{-8}$ cm)	$\langle u \rangle(10^{4}$ cm/sec)	$N^*(10^{17}$ cm)	$z(10^{7}$ sec^{-1})	$\lambda(10^{-3}$ cm)
4.2	297.35	224.21	3.6357	3.9705	1.3634	3.18	1.25
5.0	295.95	223.37	3.6382	3.9611	1.6308	3.799	1.04
6.0	296.55	223.73	3.6371	3.9631	1.9530	4.55	.87
7.0	295.25	222.95	3.6395	3.9564	2.2885	5.33	.74
10.1	295.95	223.37	3.6382	3.961	3.2942	7.67	.52

experiment, 4.2 torr, the collision rate was 3.18×10^7 sec^{-1}. When this value was used in Eq (5-7), along with a representative experimental time (40 msec), it was determined that all the atoms have undergone at least one collision. Furthermore, if it is assumed that each collision results in a de-excitation (100% efficiency), there would then be 3.18×10^7 decays/sec. This value corresponds to a radiative lifetime of 31 msec, which means that the species would not live long enough to be detected downstream from the electrodes. In other words, the radiative lifetime of the species was not on the order of the time of flight from the electrodes to the observation point. Since pulses were observed downstream from the electrodes at the representative experimental times, collisional de-excitation was not a very efficient means to depopulate the metastable states. That is, many collisions were needed to de-excite these metastable states.

VI. Conclusions

The purpose of this study was to test the validity of velocity calculations based on the plug flow assumption in flow tube applications. The plug flow velocity calculations were tested by experimentally determining the linear velocity of argon in a 5.1 cm diameter flow tube. The results were then compared to the velocity calculations based on the plug flow assumption.

Experimental verification of a fully developed laminar flow in the flow tube was obtained with gas pressures of 4.2, 5.0, 6.0, and 10.1 torr. A velocity profile characteristic of a fully developed laminar flow was constructed with the experimental velocity values. The parabolic velocity profile confirmed that large velocity gradients existed normal to the direction of flow. Therefore, the ideal state of flow called plug flow did not exist in the flow tube during the experiment.

A comparison was made between the plug flow velocities and the calculated average velocities. The results showed that the average velocity was equal to the plug flow velocity at all the operating gas pressures. Therefore, the average velocity of a gas along a flow tube centerline can be obtained by utilizing the plug flow assumption.

The parabolic velocity profile of an ideal, fully developed internal flow is described by the Poiseuille flow formula. In this formula, the linear velocity of a gas along a flow tube centerline is twice the average velocity. A comparison between the experimental and plug flow velocities showed that, on the average, the experimental velocity was $1.62 \times u_{pf}$ at a flow rate of 4576.0 standard cc/min and $1.77 \times u_{pf}$ at 5262.4 standard cc/min. Therefore, under experimental conditions, the linear gas velocity along the flow tube centerline will be somewhat less than twice the average or plug flow value since ideal laminar flow conditions are difficult to achieve. In this experiment, the presence of the electrodes in the path of flow and the presence of two cavities in the flow tube walls were the cause of lowering the ratio u_e/u_{pf}. At best, an approximation for the linear gas velocities along the centerline and at various distances from the centerline can be obtained by using the plug flow velocity in the Poiseuille flow formula, provided a laminar flow is present. This calculation will yield exact values only when a fully developed laminar flow exists in the flow tube. On the other hand, the linear velocity of a gas in a flow tube should be determined experimentally in studies where the velocity profile is not known and when the gas velocity is critical to the outcome of that study.

The afterglow technique was utilized to determine the linear velocity of argon in this study. A Stern-Volmer plot

of decay rate versus pressure was constructed from the velocity data at 5.0 torr. The results of this plot indicated the species responsible for the afterglow radiation. It was determined that the $^1D - {}^1S$ multiplet of Ar V was responsible for the afterglow. The decay rates of this metastable state of Ar V were then used to determine the effectiveness of collisional de-excitation. It was shown that collisional de-excitation was not an efficient means to depopulate the Ar V metastable state. That is, many collisions were needed to cause a transition from the metastable state to the ground state.

VII. Recommendations

The recent interest in excited state chemistry is centered on the spectroscopic and chemical examination of excited species formed in chemiluminescent reactions. Large temperature gradients affect the gas flow if the products of these reactions are studied near the reaction zone where the flame occurs. These temperature gradients can be minimized by a cooling process, thereby bringing the flow conditions close to that of plug flow. But this cooling process would affect the formation and lifetimes of these excited states. Therefore, it would be advantageous to study the validity of the plug flow assumption under the influence of large temperature gradients.

It is also advisable to study the validity of the plug flow assumption under turbulent flow conditions. The velocity profile of a turbulent flow is similar to the plug flow velocity profile. But, careful consideration must be given to longitudinal diffusion since back-mixing is a problem in turbulent flows.

Bibliography

1. Anderson, R.A., L. Hanko, and S.J. Davis. "Time Resolved Fluorescence of the $A^2\Sigma^+$ State of GeF," Journal of Chemical Physics, 68: 3286-3291 (April 1978).

2. Bradburn, G.R., R.A. Armstrong, and S.J. Davis. "Radiative Lifetime of the $A^2\Sigma^+$ State of SnF," Unpublished paper, Air Force Weapons Laboratory, Kirtland Air Force Base, New Mexico.

3. Brown, R.L. "Tubular Flow Reactors with First-Order Kinetics," Journal of Research of the National Bureau of Standards, 83: 1-8 (January 1978).

4. Capelle, Gene A. and J.M. Brom, Jr. "Reactions of Germanium Vapor with Oxidizers: Photon Yields and a New GeO Band System," Journal of Chemical Physics, 63: 5168-5176 (December 1975).

5. Capelle, Gene A., S.F. Johnson, and H.P. Broida. "Radiative Lifetime of BeO," Journal of Chemical Physics, 56: 6264-6265 (June 1972).

6. Cook, Gerhard A. Argon, Helium, and the Rare Gases, Volumes I and II. New York: John Wiley and Sons, Inc., 1961.

7. Coulson, J.M. and J.F. Richardson. Chemical Engineering, Volume Three. New York: Pergamon Press, Ltd., 1971.

8. Davis, S.J. and S.G. Hadley. "Measurement of the Radiative Lifetime of the $A^2\Sigma$ ($v'=0$) State of SiF," Physical Review A, 14: 1146-1150 (September 1976).

9. Denbigh, Kenneth. Chemical Reactor Theory, An Introduction. New York: Cambridge University Press, 1965.

10. Dixon-Lewis, G., W.E. Wilson, and A.A. Westenberg. "Studies of Hydroxyl Radical Kinetics by Quantitative ESR," Journal of Chemical Physics, 44: 2877-2884 (April 1966).

11. Felder, William and Arthur Fontjin. "High Temperature Fast-Flow Reactor Study of Sn/N_2O Chemiluminescence," Chemical Physics Letters, 34: 398-402 (July 1975).

12. Fontjin, A., W. Felder, and J.J. Houghton. "Tubular Fast-Flow Reactor Studies at High Temperatures, Kinetics of the Al/O Reaction," Chemical Physics Letters, 27: 365-368 (August 1974).

13. Fontjin, A. and S.C. Kurzius. "Tubular Fast-Flow Reactor Studies at High Temperatures. 1. Kinetics of the Fe/O_2 Reaction at 1600° K," Chemical Physics Letters, 13: 507-510 (April 1972).

14. Fontjin, Arthur, Shelby C. Kurzius, James J. Houghton, and John A. Emerson. "Tubular Fast-Flow Reactor for High Temperature Gas Kinetic Studies," Review of Scientific Instruments, 43: 726-773 (May 1972).

15. Hagar, Gordon, Richard Harris, and Steven G. Hadley. "The $a^3\Sigma^+ \rightarrow X^1\Sigma^+$ and $b^3\pi \rightarrow X^1\Sigma^+$ Band Systems of SiO and the $a^3\Sigma^+ \rightarrow X^1\Sigma^+$ Band System of GeO Observed in Chemiluminescence," Journal of Chemical Physics, 63: 2810-2820 (October 1975).

16. Hagar, Gordon, Leroy F. Wilson, and Steven S. Hadley. "Reactions of Atomic Silicon and Germanium with Nitrous Oxide to Produce Electronically Excited Silicon Monoxide and Germanium Monoxide," Chemical Physics Letters, 27: 439-441 (August 1974).

17. Kennard, Earle H. Kinetic Theory of Gases. New York: McGraw-Hill Book Co., Inc., 1938.

18. Lord Rayleigh. "Active Nitrogen of Long Duration, Law of Decay, and of Increased Brightness on Compression," Proceedings of the Royal Society of London, Series A, 151: 567-584 (June 1935).

19. Pennucci, M.A. "Parametric Evaluation of Total Pressure Loss and Recirculation - Zone Length in a Sudden Expansion Combuster," Unpublished M.S. Thesis, School of Engineering, Department of Astronautics and Aeronautics, Air Force Institute of Technology, Wright-Patterson Air Force Base, Ohio, September 1974.

20. Porter, G. (Editor). Progress in Reaction Kinetics, Volume 1. New York: Pergamon Press, Inc., 1961.

21. Rapagnani, N.L. and S.J. Davis, Chemical Laser Branch, Air Force Weapons Laboratory (Private Communication). 6 September 1979. "Program ALFA." "Program ALFA" was developed by Lockheed Missiles and Space Company, Huntsville Research and Engineering Center, Huntsville AL.

22. Roth, A. Vacuum Technology. New York: North-Holland Publishing Co., 1976.

23. Strisanov, A.R. and Sventitskii, N.S. Tables of Spectral Lines of Neutral and Ionized Atoms. New York: Plenum Data Corp., 1968.

24. Strutt, R.J. "A Chemically Active Modification of Nitrogen, Produced by the Electric Discharge," Proceedings of the Royal Society of London, Series A, 85: 219-229 (March 1911).

25. -----"A Chemically Active Modification of Nitrogen, Produced by the Electric Discharge - III," Proceedings of the Royal Society of London, Series A, 86: 262-264 (February 1912).

26. Swearengen, Peter M. "Kinetic Studies of Silicon and Germanium Oxidation Reactions," PhD Dissertation, Department of Chemistry, The University of New Mexico, December 1977.

27. Swearengen, P.M., S.J. Davis, and T.M. Niemczyk. "Reaction Rate Studies of Atomic Germanium ($^3P_{0,1}$) and Silicon (^3P_J) with Various Exodizers," Chemical Physics Letters, 55: 274-279 (April 1978).

28. Thrush, B.A. "Atom Reactions in Flow Tubes," Science, 154: 470-473 (April 1967).

29. Walas, Stanley M. Reaction Kinetics for Chemical Reactions. New York: McGraw-Hill Book Company, Inc., 1959.

30. West, J.B., R.S. Bradford, J.D. Eversole, and C.R. Jones. "Flow System for the Production of Diatomic Metal Oxides and Halides," Review of Scientific Instruments, 46: 164-168 (February 1975)

31. Wiese, W.L., M.W. Smith, and B.M. Miles. Atomic Transition Probabilities. Volume II. Sodium Through Calcium. NSRDS-NBS-22. Washington DC: National Bureau of Standards, 1969.

32. Wood, R.W. "Spontaneous Incandescence of Substances in Atomic Hydrogen Gas," Proceedings of the Royal Society A, 102: 1-9 (June 1922).

33. Wright, J.J., W.J. Spates, and S.J. Davis. "Time-Resolved Fluorescence of the $a^3\pi^+$ State of BrCl," Journal of Chemical Physics, 66: 1566-1570 (February 1977).

Appendix A

Useful Properties of Gaseous Argon

Atomic number	:	18
Atomic diameter[a], Å	:	2.95
Atomic weight	:	39.948
Density at 0° C and 1 atm, g/liter	:	1.7837
Electronic configuration	:	$1s^2\ 2s^2\ 2p^6\ 3s^2\ 3p^6$
Ionization potential[b], ev		
Lowest ionization potential (metastable)	:	11.548
Resonance potential[c]	:	11.83
First electron	:	15.759
Self-Diffusion coefficient[d] at 760 torr and 273.2°K	:	0.156 ± .002
295.2°K	:	0.178 ± .003
Viscosity[e], micropoise, at 20°C and 1 atm	:	222.86
10 atm	:	224.6
20 atm	:	226.8
25 atm	:	228.0
25°C and 1 atm	:	226.38
10 atm	:	227.9
25 atm	:	231.4

---

a (Ref 6:13), Calculated from Van der Waal's equation of state, using critical data.

b (Ref 6:237)

c Energy difference between the ground state and the lowest excited state energy level which the excited atom can return to the ground state by the emission of a photon without violating any selection rules.

d (Ref 6:203)

e (Ref 6:190)

Appendix B

Flow Regimes and the Poiseuille Flow Formula

The gas in a vacuum system can be in a viscous, molecular or intermediate state (Ref 21:60-61). Whether a gas is in the viscous, molecular or intermediate state depends on the mean free path of the molecules. The mean free path is defined as

$$\lambda = [\pi\sqrt{2}\ \sigma^2\ N^*]^{-1} \qquad \text{(B-1)}$$

where σ is the collision diameter and N^* is the number of molecules per unit volume. The collision diameter, σ, is defined as

$$\sigma = \left[\frac{\langle u\rangle\ m'}{2^{3/2}\pi\eta}\right]^{\frac{1}{2}} \qquad \text{(B-2)}$$

where $\langle u\rangle$ is the average velocity in cm/sec, m the mass in grams, and η the viscosity. When the particles have a Maxwellian velocity distribution, the average velocity is defined as

$$\langle u\rangle = \left[\frac{8\ R_o\ T}{\pi\ m}\right]^{\frac{1}{2}} \qquad \text{(B-3)}$$

where R_o is the universal gas constant, T the temperature, and m the mass in g/mole. The number of molecules per unit volume is defined as

$$N^* = \frac{N_a P}{R_o T} \tag{B-4}$$

where N_a is Avogadro's number, p the pressure, R_o the universal gas constant, and T the temperature. Substituting equations (B-2), (B-3), and (B-4) into (B-1), the mean free path is given as

$$\lambda = \left(\frac{\pi R_o T}{2 m}\right)^{\frac{1}{2}} \frac{n}{p} \tag{B-5}$$

When the mean free path of the molecules is much less than the dimensions of the vacuum enclosure, the flow is limited by viscosity. If the mean free path of the molecules is much greater than the dimensions of the vacuum enclosure, (very high vacuum), the flow is molecular. At intermediate pressures, where the mean free path of the molecules is similar to the dimensions of the vacuum enclosure, the flow is governed by viscosity as well as molecular phenomena. This is the intermediate flow regime. The limit between the viscous, molecular, and intermediate flow regimes is described by the value of the Knudsen number. (Table XIV). The Knudsen number is defined as

$$Kn = D/\lambda \qquad \text{(B-6)}$$

where D is the diameter of the tube, and λ the mean free path.

In the range where the state of the gas is viscous, the flow can either be turbulent or laminar. The limit between turbulent and laminar flow is defined by the value of the Reynolds number. The Reynolds number, a dimensionless quantity, is defined as

$$Re = (\rho\ u\ D) / \eta \qquad \text{(B-7)}$$

where ρ is the density of the gas, u the velocity, D the diameter of the tube, and η the viscosity. Table XIII summarizes the flow regimes.

When the flow is viscous and laminar in a long tube of circular cross-section, the velocity distribution is expressed by Poiseuille's equation for laminar flow. This equation is derived by considering a uniform circular cross-section with radius R as shown in Figure 15(a). In this development, it is assumed that the mean velocity component of the molecules in the direction of flow is a function only of the distance, y, from the centerline. Thus, the boundary conditions are established:

Table XIII

Flow Regimes

State of the Gas	Flow Regime	Condition
Viscous	Turbulent	Re > 2300 Kn > 110
	Laminar	Re < 2300 Kn > 110
Transition	Intermediate	1 < Kn < 110
Rarefied	Molecular	Kn < 1

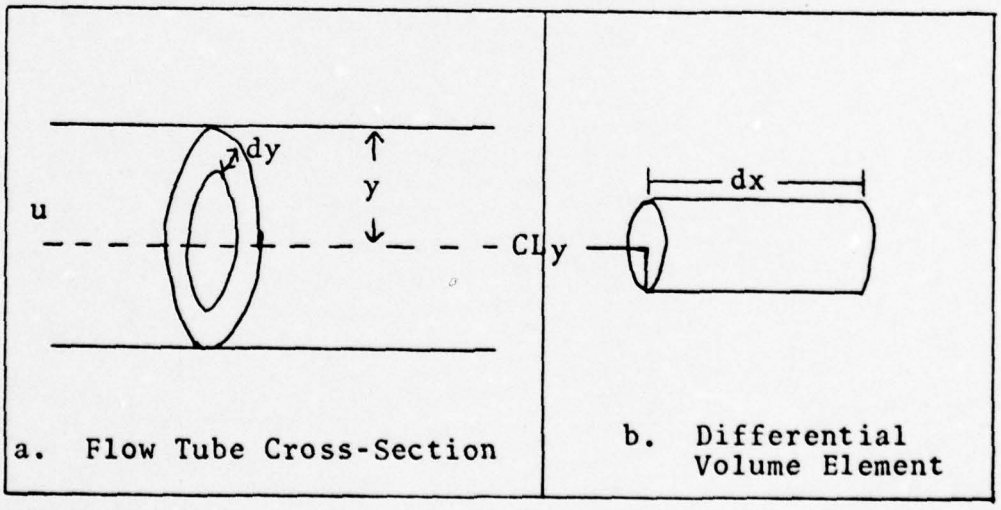

Figure 15. Flow Tube Cross-Section and Differential Volume Element

$$u = 0 \quad \text{at} \quad y = R \tag{B-8a}$$

$$u = u_{max} \quad \text{at} \quad y = 0 \tag{B-8b}$$

The gas molecules entering a differential volume element of length dx (Figure 15(b)) experience a shearing stress due to viscous forces. The shearing stress is given as

$$\tau = \eta(\partial u/\partial y) \quad , \quad \partial u/\partial y < 0 \tag{B-9}$$

where η is the viscosity and $\frac{\partial u}{\partial y}$ the velocity gradient. Then, the viscous drag on a curved surface is defined as

$$\tau = 2\pi y \, dx \, \eta(\partial u/\partial y) \tag{B-10}$$

A pressure difference in this volume element will produce a force that acts on the fluid. If a steady flow is present in this volume element, the force due to the pressure difference is balanced by the viscous drag over the curved surface. This is stated as

$$2\pi y \, dx \, \eta(\partial u/\partial y) + \pi y^2 \, dp = 0 \tag{B-11}$$

Therefore,

$$\frac{\partial u}{\partial y} = -\left(\frac{y}{2\eta}\right)\frac{dp}{dx} \qquad \text{(B-12)}$$

Integrating Eq (B-12) and solving for u with the boundary conditions (B-8a) and (B-8b), the Poiseuille flow formula becomes

$$u = \left(\frac{y^2 - R^2}{4\eta}\right)\frac{dp}{dx} \qquad \text{(B-13)}$$

Equation (B-13) can be written in terms of the average velocity, u_{av} . The average velocity is defined as

$$u_{av} = \dot{V} / A \qquad \text{(B-14)}$$

where $\dot{V}$ is the volumetric flow rate, and A the cross-sectional area. The volumetric flow rate is defined as

$$\dot{V} = \int u\, dA = \int_0^R u\,(2\pi y\, dy) \qquad \text{(B-15)}$$

Integrating (B-15) and substituting the expression for u as defined in Eq (B-13), the volumetric flow rate is expressed as

$$\dot{V} = \frac{-\pi R^4}{8\eta}\frac{dp}{dx} \qquad \text{(B-16)}$$

Therefore, substituting Eq (B-16) into Eq (B-14), the average velocity is written as

$$u_{av} = \frac{\dot{V}}{\pi R^2} = \frac{-R^2}{8\eta} \frac{dp}{dx} \tag{B-17}$$

Thus, the Poiseuille flow formula, written in terms of the average velocity, is

$$u = 2\, u_{av} \left[1 - \frac{y^2}{R^2}\right] \tag{B-18}$$

This formula shows the characteristic parabolic profile of laminar flows in cylindrical tubes.

An expression for the pressure drop in a cylindrical tube caused by viscous forces can be obtained by considering the number of molecules or atoms that flow in a cylindrical shell between r and r+dr (Ref 28:105-108). The differential flow rate molecules is given by

$$dF = (nu)\, 2\pi y\, dy \tag{B-19}$$

where n is the number of molecules or atoms per unit volume. Substituting Eq (B-13) into (B-19), the total flow rate is given as

$$F = n\int_0^R u\, 2\pi y\, dy = \frac{2\pi n}{4\eta} \frac{dp}{dx} \int_0^R y(R^2 - y^2)\, dy \tag{B-20}$$

Integrating and using the ideal gas law in the form

$$\frac{n}{V} = P / kT \qquad \text{(B-21)}$$

the flow rate becomes

$$F = \frac{\pi R^4 p}{8\eta kT} \frac{dp}{dx} \qquad \text{(B-22)}$$

Now,

$$F\int_0^L dx = \frac{\pi R^4}{8\eta kT} \int_{p_1}^{p_2} p\, dp \qquad \text{(B-23)}$$

where L is the length of the tube, p_1 the upstream pressure, and p_2 the downstream pressure. Thus, the number of molecules flowing per unit time is

$$F = \frac{\pi R^4 \bar{p} \Delta p}{8\eta kTL} \qquad \text{(B-24)}$$

where $\bar{p} = (p_2 + p_1)/2$ and $\Delta p = p_2 - p_1$. Rearranging (B-24) and multiplying by Avogadro's number, the pressure drop can be calculated using

$$p_2^2 - p_1^2 = \frac{16F'L\, R_o T}{R^4 \pi} \qquad \text{(B-25)}$$

where F' is the flow rate in moles/sec.

For example, if argon is flowing in a cylindrical tube, 5.1 cm in diameter and 200 cm in length, the mean free path is calculated according to Eq (B-5). At a gas pressure of 10 torr (p_1) and a temperature of 293° K, $= 5.2 \times 10^{-4}$ cm. Therefore, the value of the Knudsen number is 9.8×10^3 which means that the flow is viscous. The viscosity of argon at 293° K is 221.7 micropoise and, with a linear velocity of 10^3 cm/sec, the value of the Reynold's number is 501.6. Since the Reynold's number is less than 2300, the flow is laminar. To calculate the upstream pressure in the cylindrical tube, Eq (B-25) is used. With a flow rate of 5.46×10^{-3} mole/sec ($\dot{V} = 10^4$ cm^3/sec), the pressure upstream, p_2, is 9.999931743 torr. This corresponds to a pressure difference due to viscosity of 6.83×10^{-5} torr.

Appendix C

Flow Tube Pictures

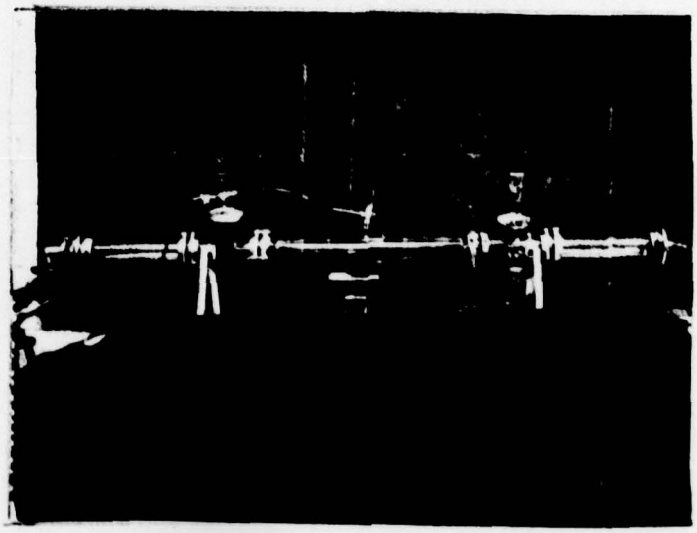

a. Flow Tube

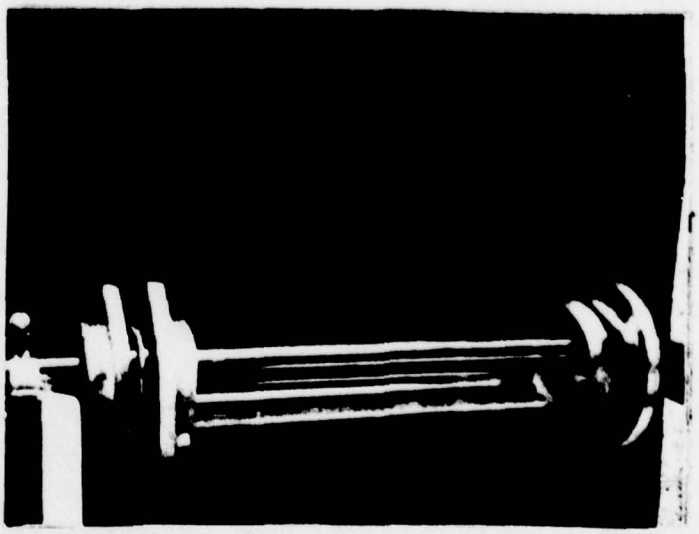

b. Flow Inlet Section

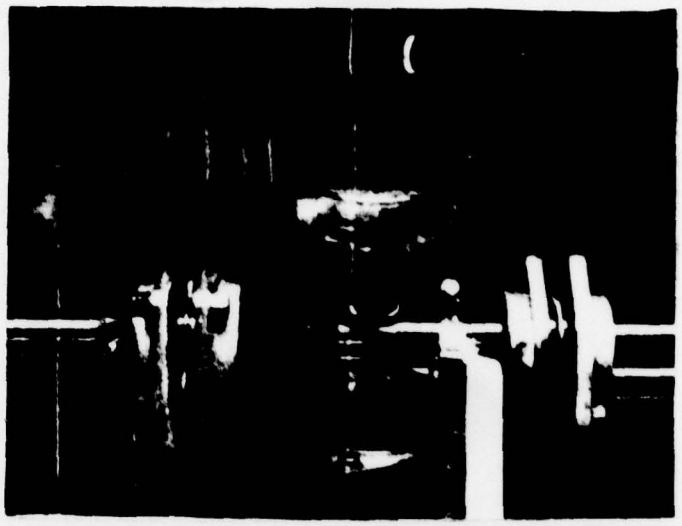

c. Discharge Section

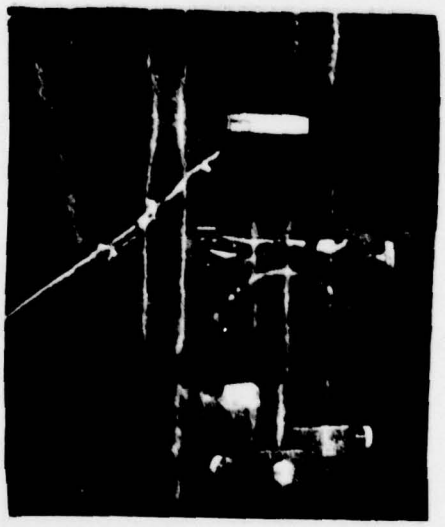

d. PMT System (Front)

e. PMT System (Side)

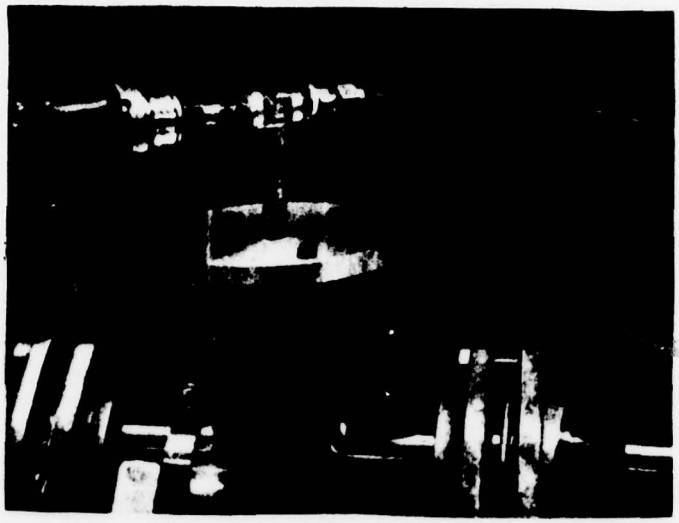

f. Pressure Measurement Section

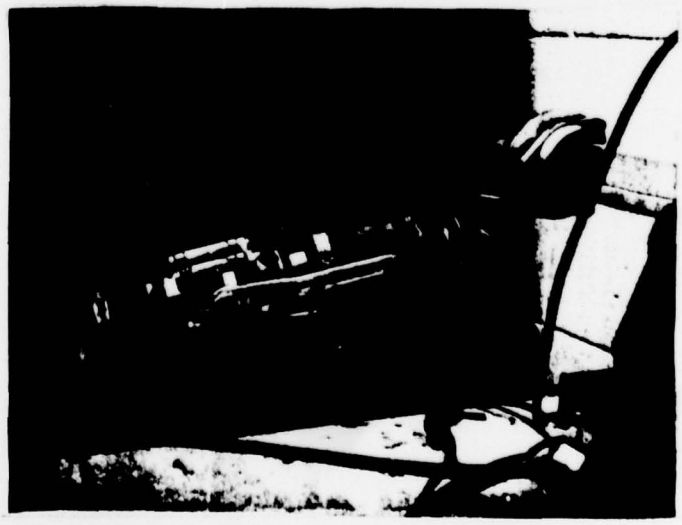

g. Flow Outlet Section

Appendix D

Sample Photographic Data

These pictures are samples of the data obtained at a gas pressure of 4.2 torr and a flow rate of 4576 std cc/min. The distance, x , from the electrodes to the observation point is labeled below each photograph. The time scale is plotted on the x-axis and is 20 msec per five lines, while the y-axis records the intensity of each pulse. The solid line in each picture is the positive portion of the square wave that triggered the spark discharge. This line was used as a time reference; that is, the time was counted beginning at the point where the square wave triggered the discharge. The time decaying line on the left side of each pulse was the reflected signal of the discharge off the inner flow tube walls.

a. x = 26.9 cm

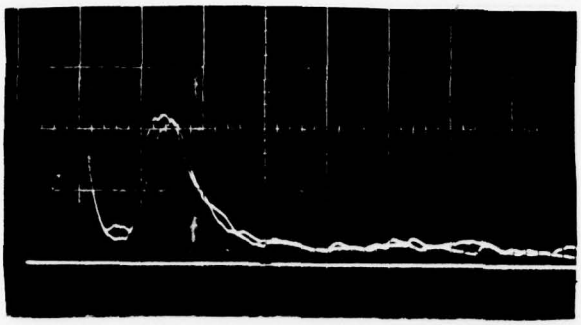

b. x = 37.1 cm

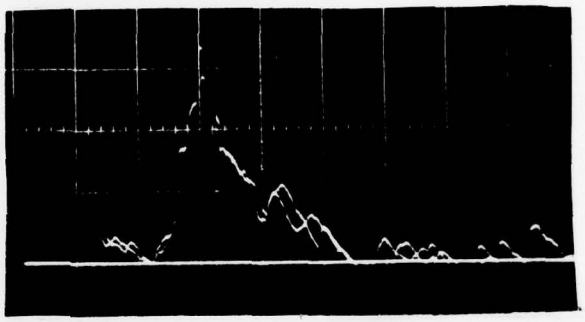

c. x = 47.0 cm

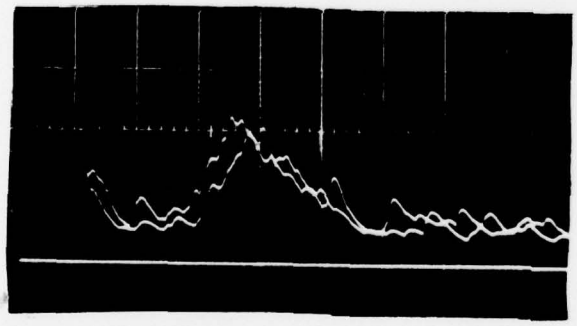

d. x = 57.4 cm

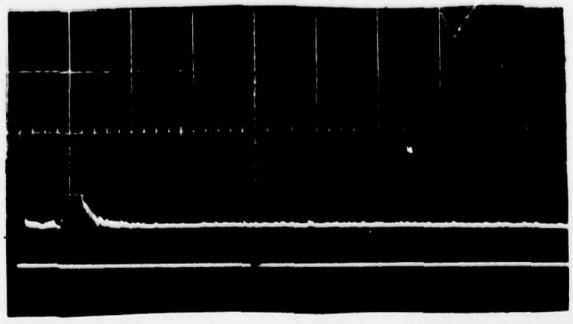

e. x = 69.9 cm

Appendix E

Experimental Raw Data

The linear velocity of argon was determined with the following experimental data.

1. p (gas) = 4.2 torr, p (atm) = 740.1 mm Hg
   T (atm) = 24.2° C , $\dot{V}$ = 4576 std cc/min

x (cm)	t (msec)
0.0	0,0,0,0,0
	0,0,0,0,0
16.9	13,13,12
	14,14,12
26.9	25,22,23,22,23
	23,24,24,22,22
37.1	30,34,33,32,32
	34,32,31,33,32
47.0	41,41,39,43,41
	43,42,42,40,41
57.4	57,53,49,48,54
	53,52,58,57

2. p (gas) = 5.0 torr, p (atm) = 736.4 mm Hg
T (atm) = 22.8° C , $\dot{V}$ = 5262.5 std cc/min

x (cm)	t (msec)
0.0	0
26.9	15.0
31.9	21.0
37.1	28.5
42.1	32.5
47.0	35.5
52.0	45.0
56.9	48.8

3. p (gas) = 6 torr, p (atm) = 740.1 mm Hg
T (atm) = 23.4° C, $\dot{V}$ = 4576 std cc/min

x (cm)	t (msec)
0.0	0,0,0,0,0
	0,0,0,0,0
16.9	21,20,21
	21,21,17
26.9	25,27,33,29,29
	25,32,30,31,30
37.1	49,48,39,47,45
	49,47,41,49
47.0	61,65,51,57,67
	66,65,65,64,62
57.4	71,71,59,60,69
	75,73,73,81

4. p (gas) = 10.1 torr, p (atm) = 736.4 mm Hg
T (atm) = 22.8° C , $\dot{V}$ = 5262.4 std cc/min

x (cm)	t (msec)
0.0	0.0
26.9	42.0
31.9	56.5
33.9	65.0

Appendix F

Collision Parameters[a]

In a pure gas, the average number of collisions per second, z, experiences by a single molecule or atom is given by

$$z = \langle u \rangle / \lambda \tag{F-1}$$

where λ is the mean free path and $\langle u \rangle$ is the average speed of the atom or molecule. When the gas is described by a Maxwellian distribution, the average speed is defined as

$$\langle u \rangle = \left[\frac{8 R_o T}{\pi m}\right]^{\frac{1}{2}} \tag{F-2}$$

where R_o is the universal gas constant, T the temperature, and m the atomic mass.

The mean free path, λ, is defined in Eq (F-3).

$$\lambda = [\pi\sqrt{2}\ \sigma^2\ N^*]^{-1} \tag{F-3}$$

where σ is the collision diameter and N^* the total number of atoms per unit volume. Substituting (F-3) into (F-1), the expression for the average number of collisions per second becomes

---

[a] (Ref 17: 98-104)

$$z = \sqrt{2}\ \pi\ \sigma^2 \langle u \rangle\ N^* \qquad \text{(F-4)}$$

The collision parameter, , can be calculated using

$$\sigma = \frac{\langle u \rangle\ m'}{2^{3/2} \pi \eta}^{\frac{1}{2}} \qquad \text{(F-5)}$$

where η is the viscisoty and m' the mass in grams. The total number of atoms per unit volume is determined from

$$N^* = \frac{N_a\ p}{R_o\ T} \qquad \text{(F-6)}$$

where N_a is Avogadro's number and p the pressure.

For example, the mean speed of argon atoms at 5 torr and 293° K is 3.9×10^4 cm/sec . At 293° K, the viscosity of argon is 221.7 micropoise. Therefore, the collision parameter is 3.6×10^{-8} cm and the number of atoms per unit volume at 5 torr is 1.7×10^{17} . Thus, the number of collisions per second is 3.6×10^7 .

AD-A080 179 AIR FORCE INST OF TECH WRIGHT-PATTERSON AFB OH SCHOO--ETC F/G 7/4
THE VALIDITY OF VELOCITY CALCULATIONS BASED ON THE PLUG FLOW AS--ETC(U)
DEC 79 P J WOLF
UNCLASSIFIED AFIT/GEP/PH/79D-14 NL

2 OF 2
AD
A080179

END
DATE
FILMED
3-80
DDC

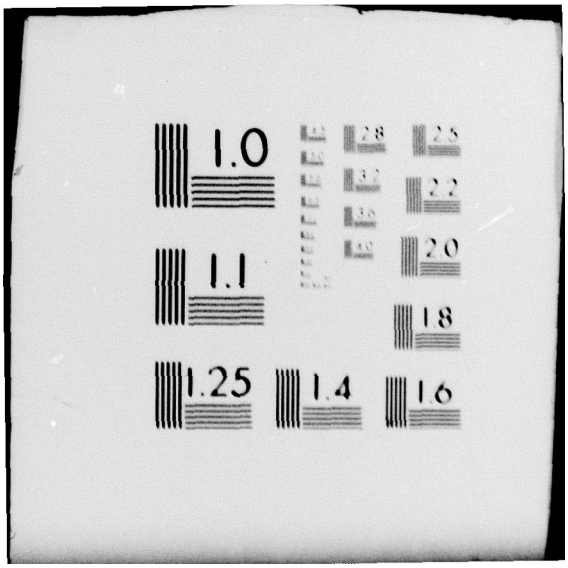
1.0
1.1
1.25
1.4
1.6
2.8
3.2
3.6
4.0
2.5
2.2
2.0
1.8

Vita

Paul James Wolf was born on 31 May 1956 at Ashyia Air Force Base, Kyushu, Japan. He graduated from Saint Peter's Preparatory High School in Jersey City, New Jersey in 1974. He attended Regis College in Denver, Colorado, from which he received the degree of Bachelor of Science in physics in May 1978. Upon graduation, he received a commision in the United States Air Force through the ROTC program at the University of Colorado in Boulder, Colorado. He then entered the School of Engineering, Air Force Institute of Technology, in June 1978.

Permanent Address: 770 Second Street
Secaucus, NJ 07094

UNCLASSIFIED

SECURITY CLASSIFICATION OF THIS PAGE (When Data Entered)

REPORT DOCUMENTATION PAGE		READ INSTRUCTIONS BEFORE COMPLETING FORM
1. REPORT NUMBER AFIT/GEP/PH/79D-14	2. GOVT ACCESSION NO.	3. RECIPIENT'S CATALOG NUMBER
4. TITLE (and Subtitle) THE VALIDITY OF VELOCITY CALCULATIONS BASED ON THE PLUG FLOW ASSUMPTION IN FLOW TUBE APPLICATIONS		5. TYPE OF REPORT & PERIOD COVERED M.S. Thesis 6. PERFORMING ORG. REPORT NUMBER
7. AUTHOR(s) Paul J. Wolf 2d Lt USAF		8. CONTRACT OR GRANT NUMBER(s)
9. PERFORMING ORGANIZATION NAME AND ADDRESS Air Force Institute of Technology (AFIT-EN) Wright-Patterson Air Force Base OH 45433		10. PROGRAM ELEMENT, PROJECT, TASK AREA & WORK UNIT NUMBERS
11. CONTROLLING OFFICE NAME AND ADDRESS Air Force Institute of Technology (AFIT-EN) Wright-Patterson Air Force Base OH 45433		12. REPORT DATE December 1979 13. NUMBER OF PAGES 94
14. MONITORING AGENCY NAME & ADDRESS(if different from Controlling Office)		15. SECURITY CLASS. (of this report) UNCLASSIFIED 15a. DECLASSIFICATION/DOWNGRADING SCHEDULE

16. DISTRIBUTION STATEMENT (of this Report)

Approved for Public Release; Distribution Unlimited

17. DISTRIBUTION STATEMENT (of the abstract entered in Block 20, if different from Report)

18. SUPPLEMENTARY NOTES

Approved for Public Release; IAW AFR 190-17

JOSEPH P. HIPPS, Major, USAF
Director of Public Affairs

19. KEY WORDS (Continue on reverse side if necessary and identify by block number)

Flow Tube	Velocity Profile
Velocity Measurements	Radiative Lifetime
Argon Afterglow	Plug Flow Assumption

20. ABSTRACT (Continue on reverse side if necessary and identify by block number)

The validity of linear velocity calculations based on the plug flow assumption were tested on flowing argon at 4.2, 5.0, 6.0, and 10.1 torr. The linear velocity of argon was experimentally determined along the centerline of a flow tube, using the argon afterglow technique. It was found that the linear velocity was 1.62 times the plug flow (average) velocity at a flow rate of 4576.0 standard cc/min and 1.77 times the plug flow velocity at 5262.4 standard cc/min. The velocity data taken at various distances from the centerline

DD FORM 1 JAN 73 1473 EDITION OF 1 NOV 65 IS OBSOLETE

UNCLASSIFIED

SECURITY CLASSIFICATION OF THIS PAGE (When Data Entered)

ITEM 20 (Cont'd)

revealed a fully developed laminar flow. The velocity results differed from that predicted by the Poiseuille flow formula, and it was determined that this difference was mainly due to obstructions in the argon flow. It was concluded that the plug flow assumption can be used to obtain linear gas velocities in a fully developed laminar flow and approximate gas velocities if the laminar flow is not fully developed. A Stern-Volmer plot was constructed and the results indicated that the $^1D - {}^1S$ multiplet of Ar V was responsible for the afterglow.

$(1)D \quad (1)S$